Effect of Glass Formation-Thin Films

Kathleen Richardson

Clemson University

richar3@clemson.edu
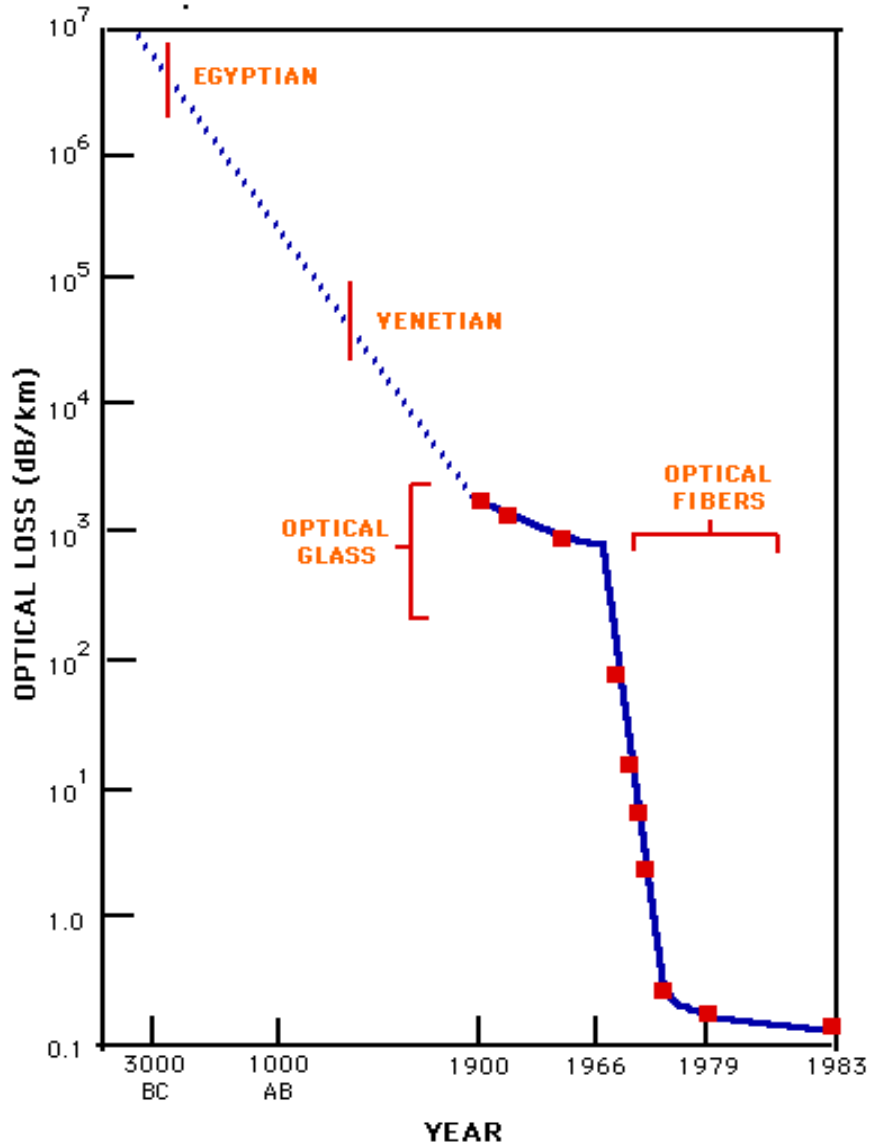
Glass – ancient transmission medium
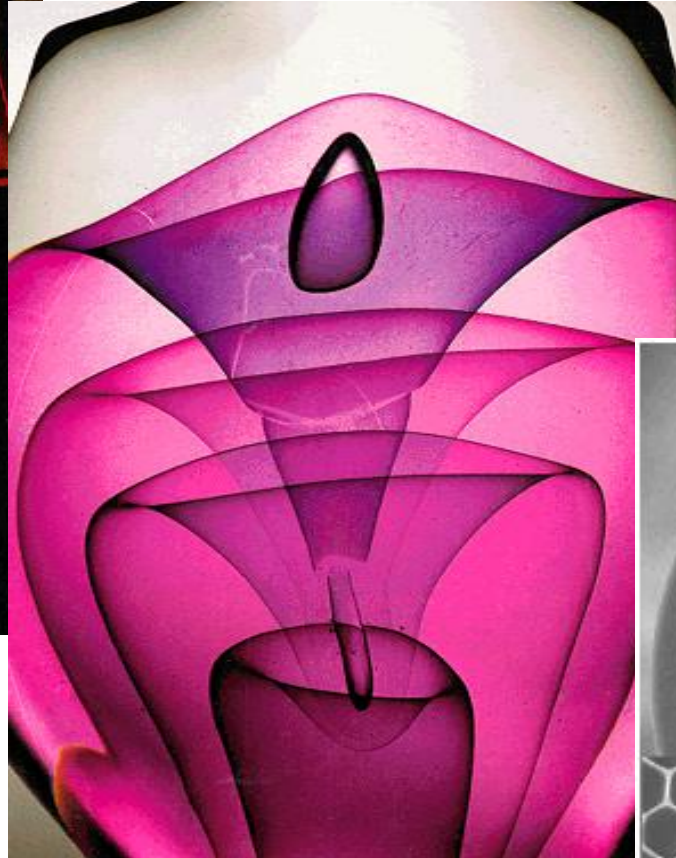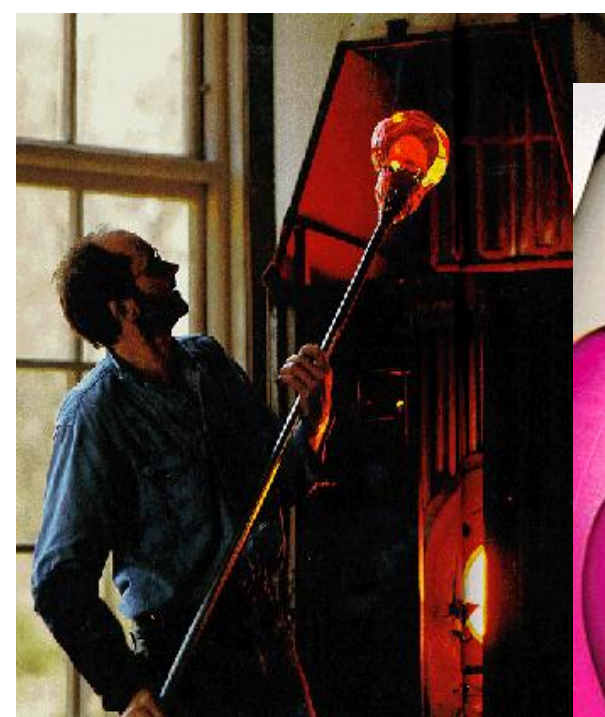

Photo courtesy of the Optoelectronics Research Centre (ORC) at the University of Southampton, UK
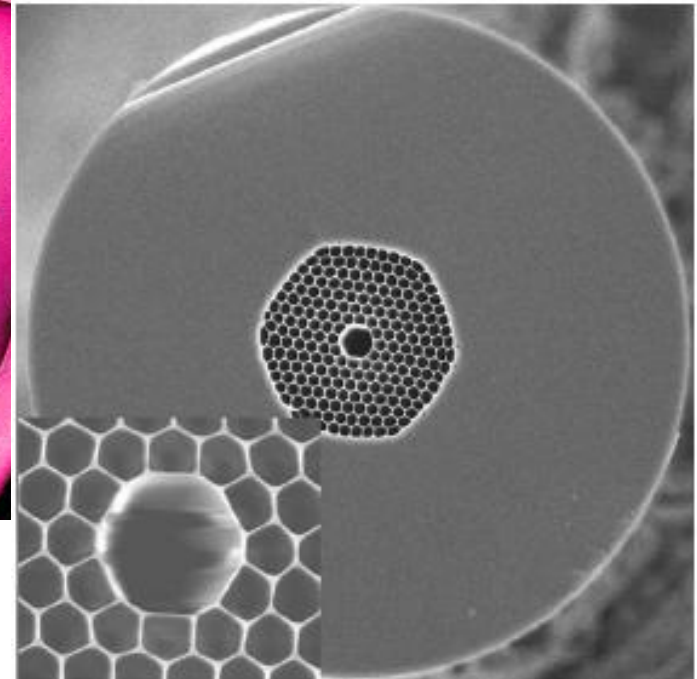

…..beauty can have function too!

http://people.deas.harvard.edu/~jones/ cscie129/nu_lectures/lecture10/images/fo_abs.html

Its not just what its made of…

Photos courtesy of National Geographic (left) and the Optoelectronics Research Centre (ORC) at the University of Southampton, UK (below)

…its the secret of the manufacturing technology that makes the final part unique and functional ….

Processing history dictates properties

Formation-induced attributes dictate the form, performance and lifetime on a resulting glass part. Here, residual stress frozen into a Prince Rupert's drop during its formation (which appears as birefringence under crossed polarizers) ultimately limits the drop's mechanical stability and life.
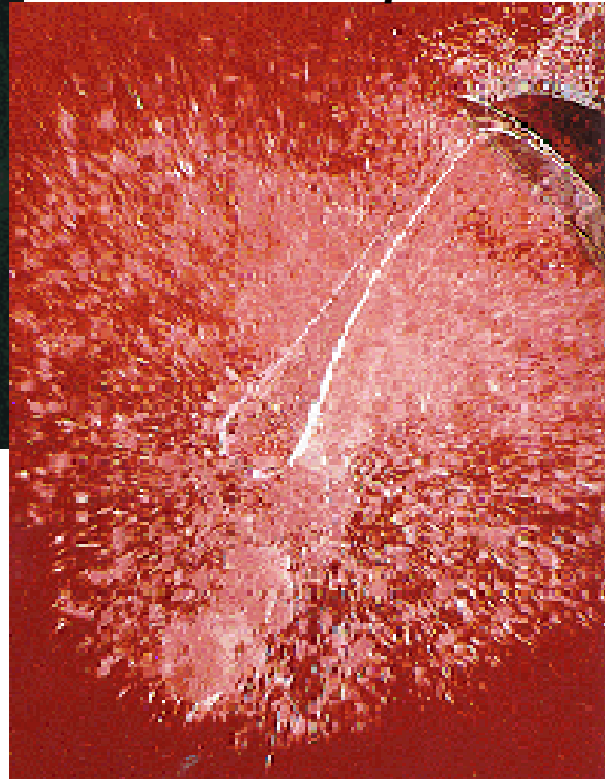
*Photos courtesy of National Geographic*

Outline

- Formation of glassy films – the basics
  - Vapor deposition
    - CVD
    - PLD
  - Thermal Evaporation
  - RF Sputtering
  - Others: e⁻ beam deposition, ion beam assist, sol gel
- Amorphous versus non-crystalline films
- Effect of processing parameters
- Defects and damage
- Characterization tools
- Bulk/film variations

Volume versus Temperature Plot
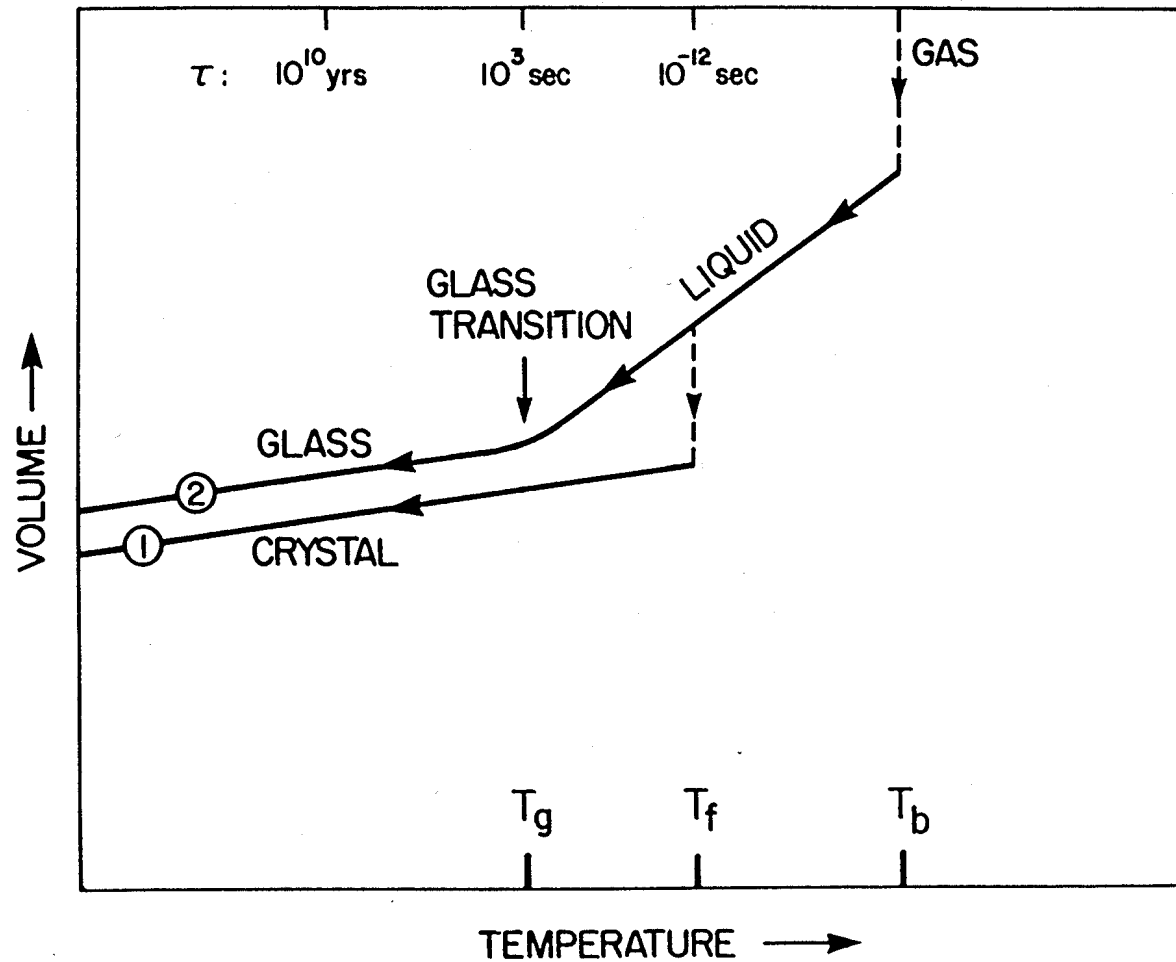
Viscosity Temperature curve
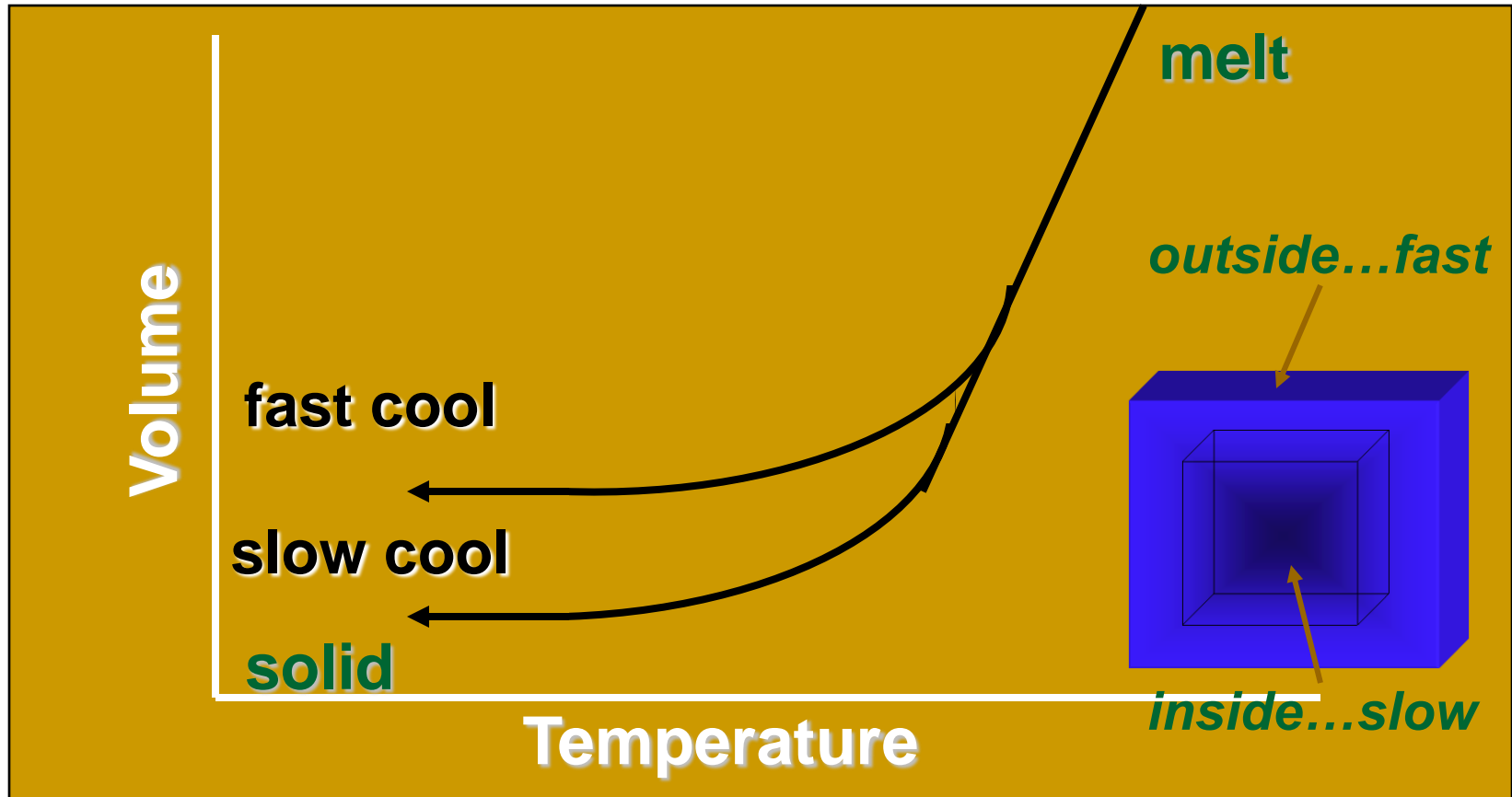
Difference in cooling rates--> stress outside (compression), inside (tension)

Schematic Sketches of the Atomic Arrangements in Solids

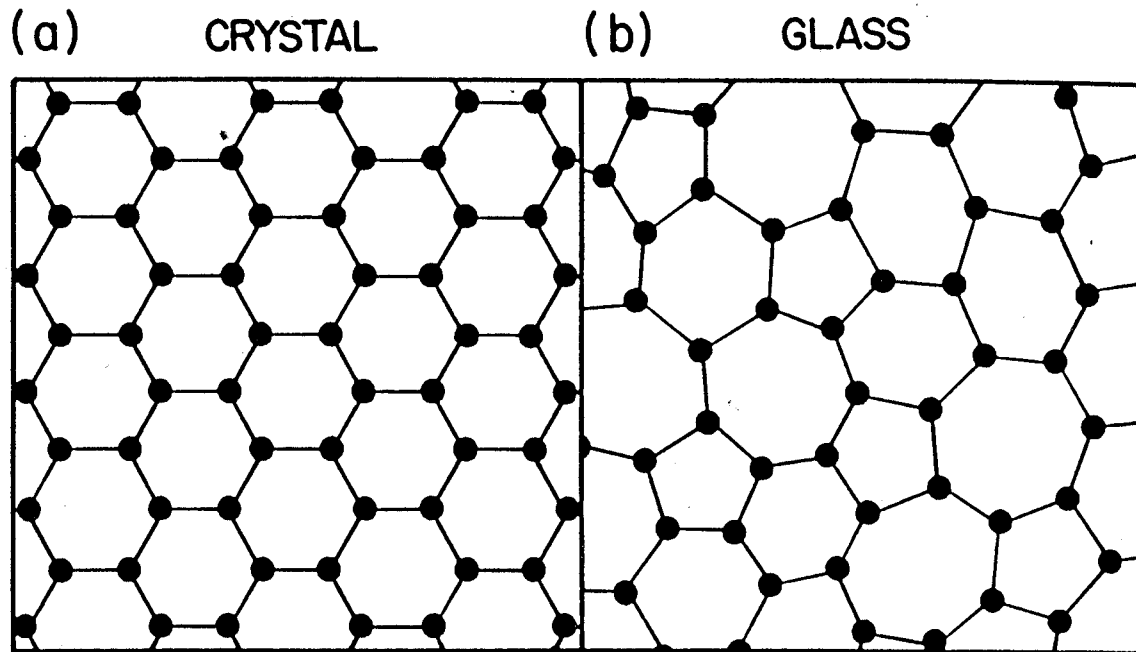(a) CRYSTAL   (b) GLASS

Schematic of the Radial Distribution Functions

CRYSTAL   GLASS

(a)   (b)
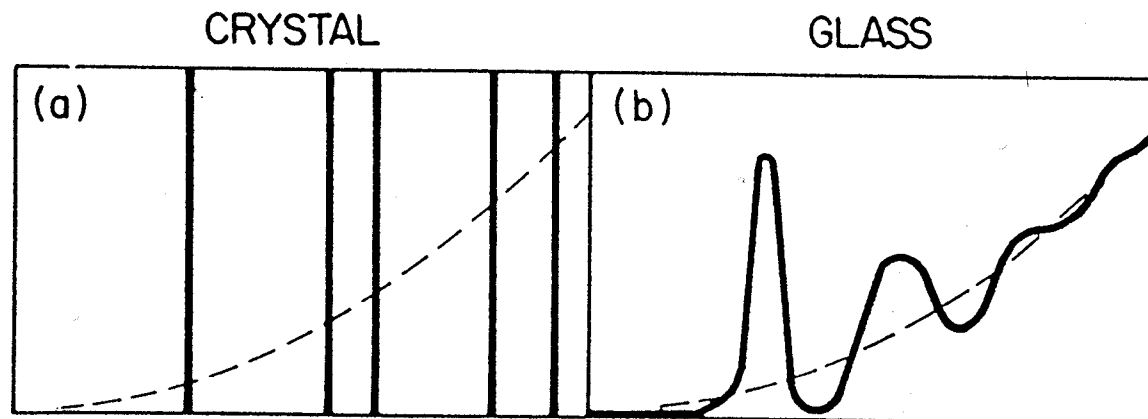
Viscosity-Temperature curve – film deposition

melt

Film surface

Volume

fast cool

slow cool

solid

Temperature

substrate
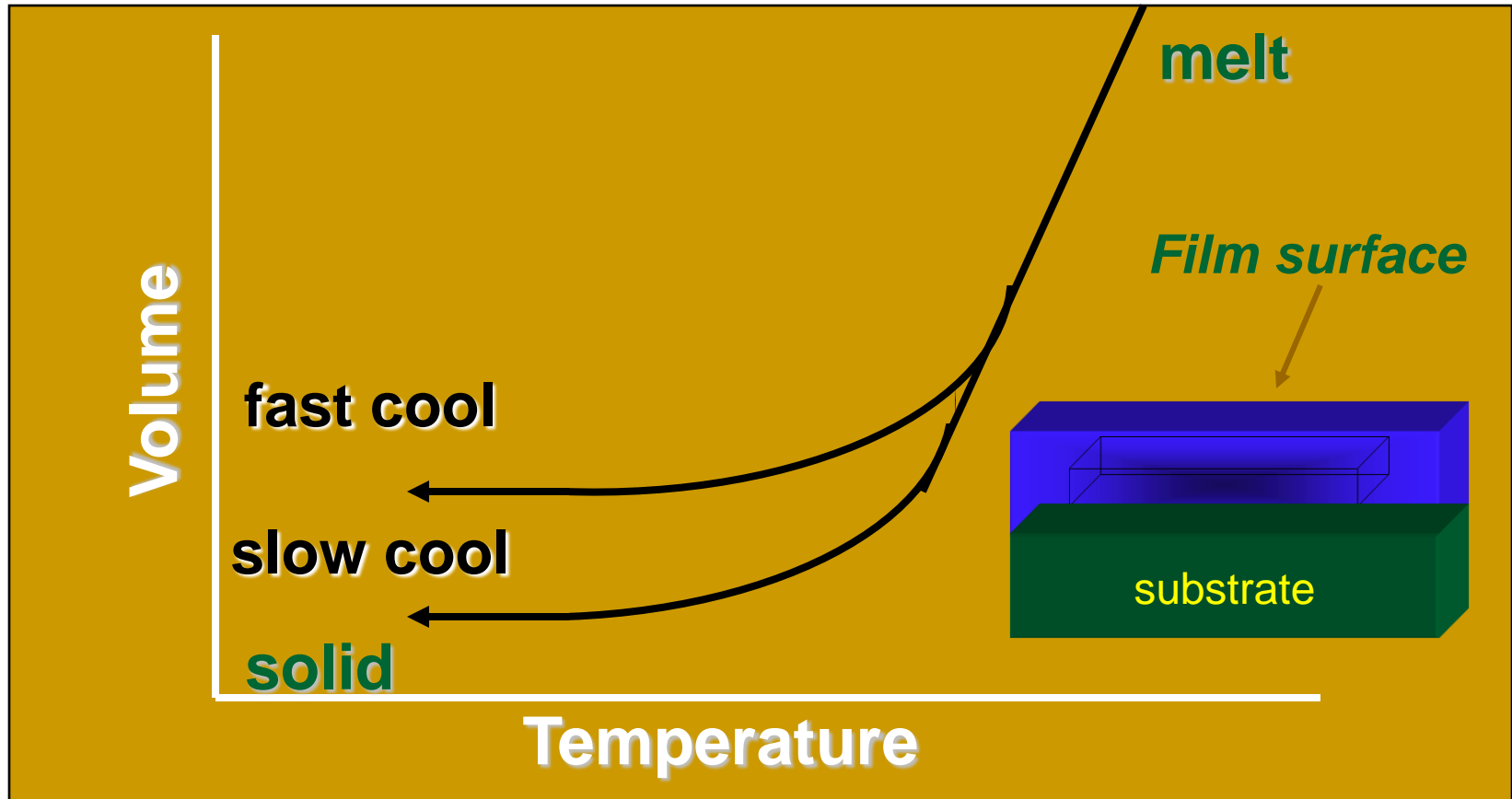
Difference in cooling rates leads to

- *stress, anisotropy (Δn, $\Delta\rho$, ΔTg, $\Delta bonding$),*
relaxation rates

Bulk optical glass manufacturing process

- **Batching**
- **Melting**
- **Refining**
- **Stirring**
- **Forming**
- **Annealing**
- **Relaxation to equilibrium**
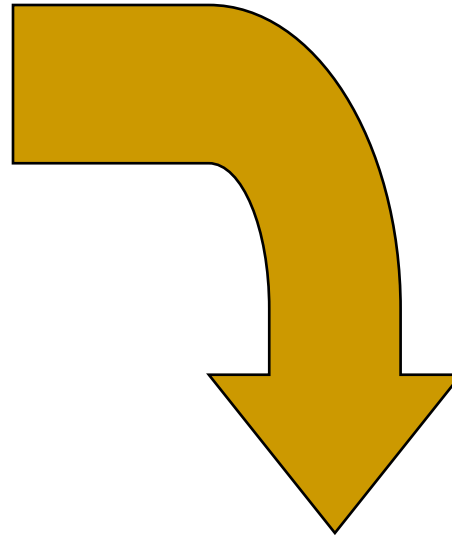
Thin film glass manufacturing process

- **Target processing**
- **Deposition (means of energy deposition influences residual "stored energy")**
- **Annealing**
- **Relaxation to equilibrium**

Type of deposition influences structure

- Heating rate analogy

- Higher energy process creates glass structure "further" from equilibrium

- Glass film structure is "further" from that of parent bulk glass

- Stability of film structure over time influenced by distance from equilibrium

Deposition rate ~ condensation rate
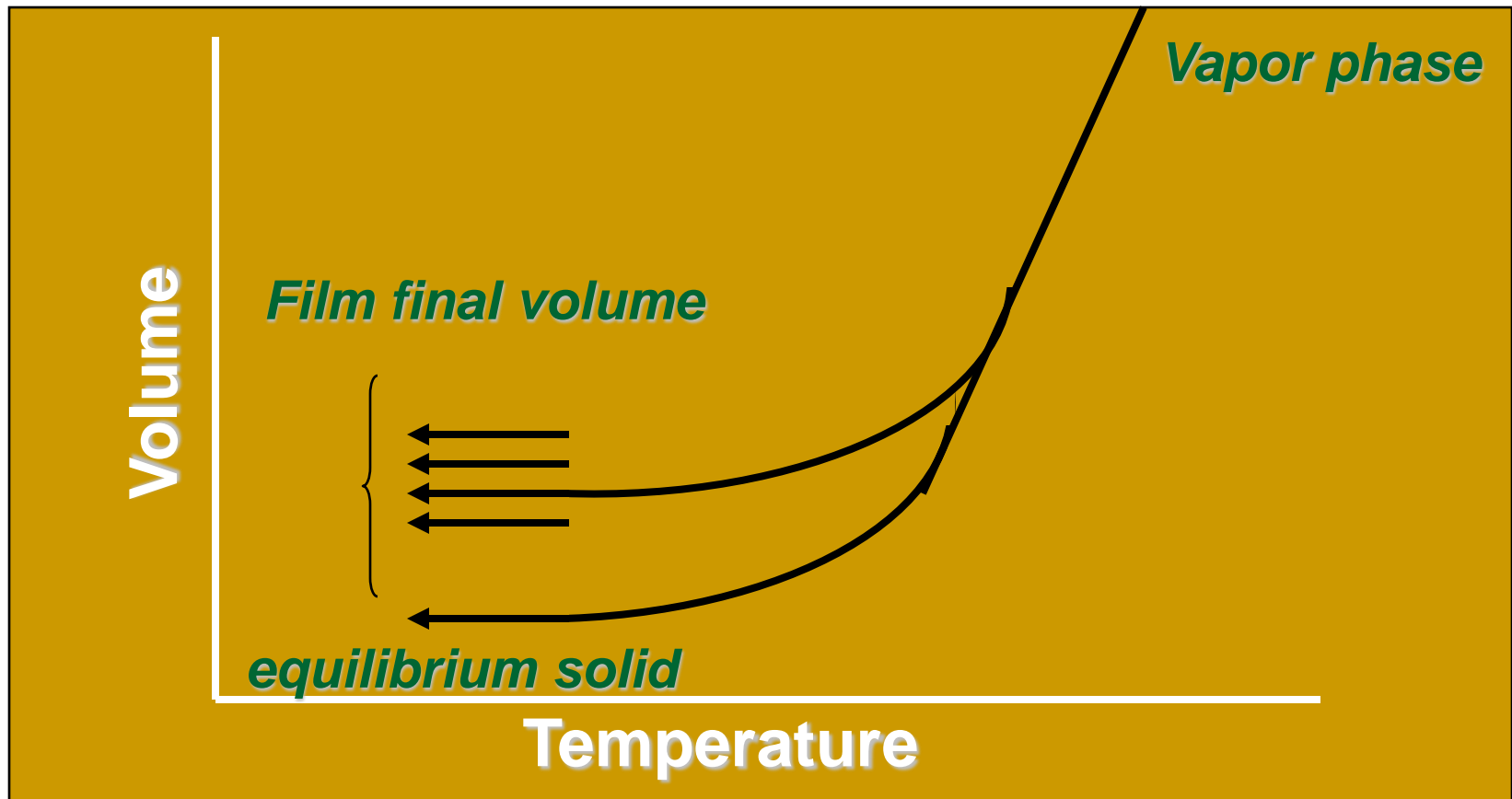
Final film volume dictates film properties and stability

Films – key issues

- ## Maintaining compositional similarity
  - Bulk-film properties vary when thermal history varies
  - Compositional variation (from the vapor or plasma phase)
    - Vapor phase > variation than plasma
    - Preferential target removal
      - variation in vapor pressures
    - Preferential film condensation
      - Molecular units present in vapor or plasma may be "fragments of structural units" OR "clusters of structural units"
  - Structural variation
    - Results from composition and condensation rate differences

Film Deposition Techniques
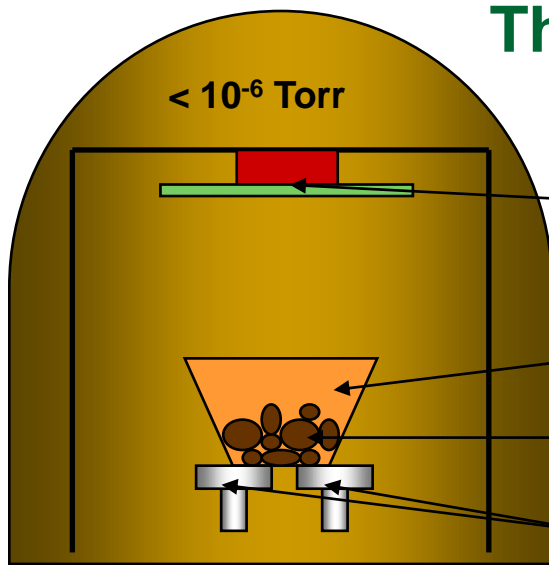
Thermal Evaporation

Pulsed Laser Deposition

< 10^{-6} Torr

Substrate (Glass/Si)

Molybdenum Boat

Bulk Glass Target

Target heaters

Laser beam

Port with quartz window

Target carousel
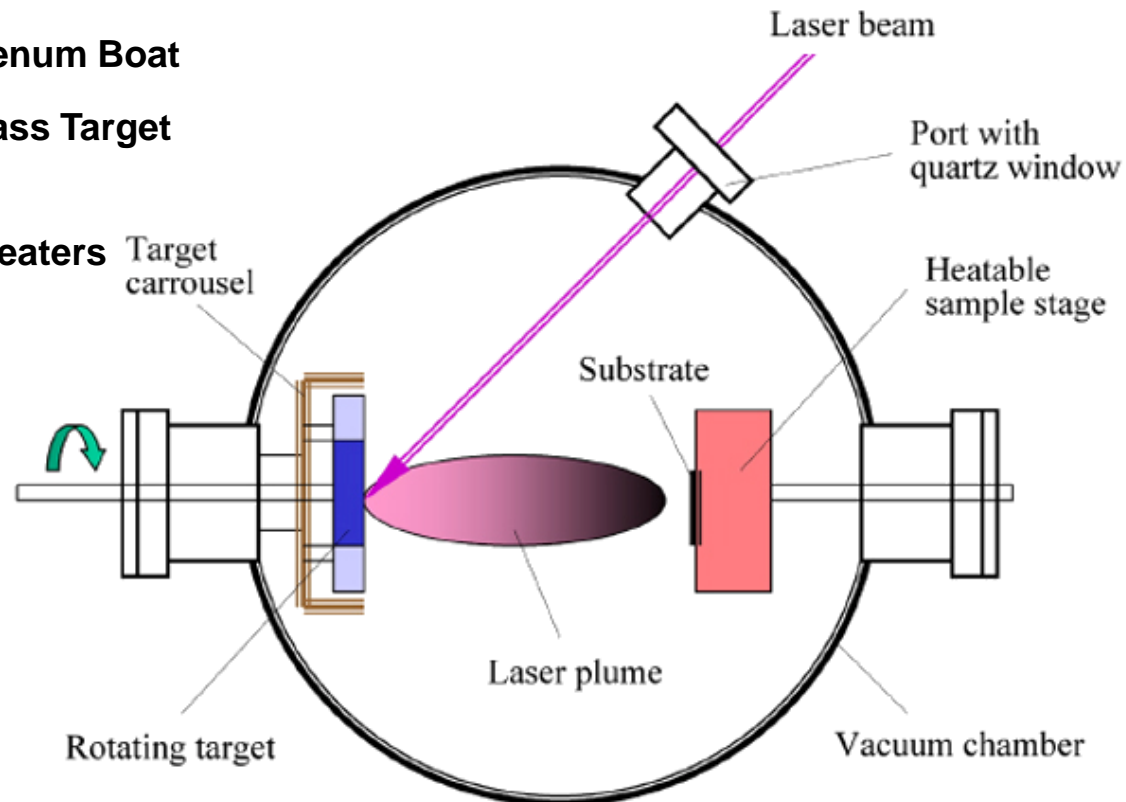
Heatable sample stage

Substrate

Rotating target

Laser plume

Vacuum chamber

Targets for deposition

- **Bulk glass can be utilized as starting "parent" glass**

$GeO_2 - Na_2B_4O_7$

$GeO_2 - Sb_2O_3 - B_2O_3$

$GeO_2 - NaPO_3$

$GeO_2 - Sb_2O_3$

Melting
t=30min

Quenching

Annealing
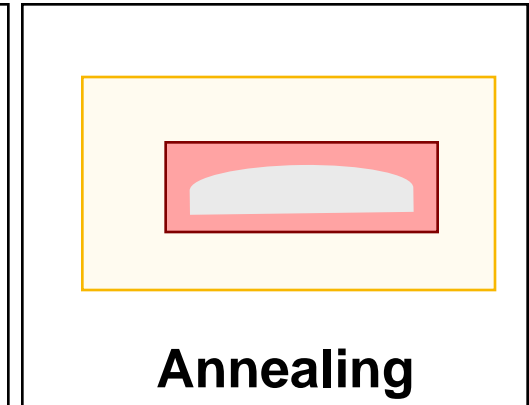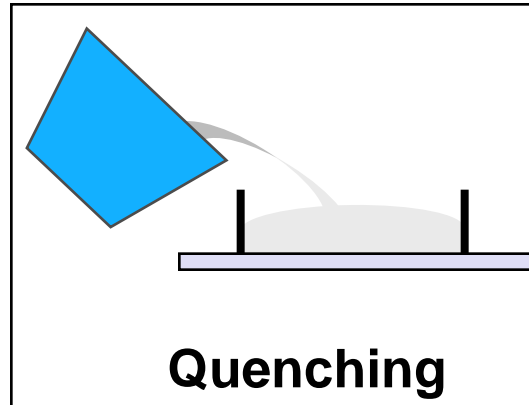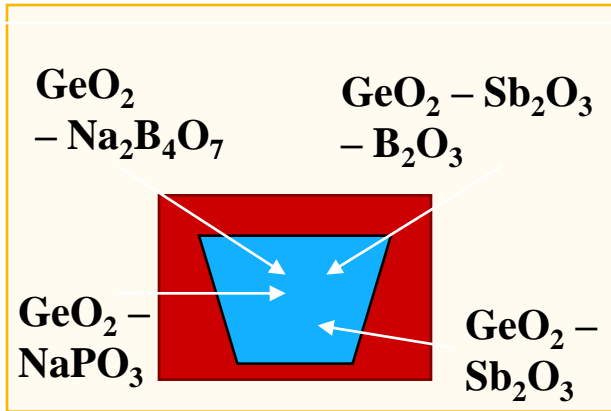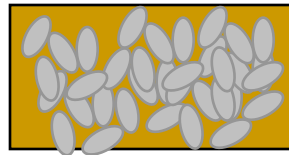
Crush to form pieces of target glass

Polished bulk piece of glass

Film Deposition Techniques - Targets

- **Single component targets**
  - Good chance at maintaining stoichiometry
  - Deposition environment (Ar, O_2, air) influences
- **Bi-component targets**
  - Some variation may result due to variation in constituent properties (Tm, vapor pressure, etc)
  - Stabilty versus crystallization depends on similarity
- **Multi-component targets**
  - Selectivity of deposition rate can result in non-uniform film
  - Preferential deposition rates can lead to graded properties
    - Near-substrate properties ≠ top of film properties ≠ bulk glass properties
  - Target fabrication technique is crucial
    - Uniformity in target composition yields higher probability of uniform film → structure and properties

Target fabrication

- Multi-component glass: oxide/oxy-sulfide

Melting
t=30min

GeO$_2$ – Na$_2$B$_4$O$_7$

GeO$_2$ – Sb$_2$O$_3$ – B$_2$O$_3$

GeO$_2$ – NaPO$_3$

GeO$_2$ – Sb$_2$O$_3$

Quenching

Annealing

H$_2$S Flow
50 C below the Tg

Pulverize to form a powder

Sulfination

Press to form pellet target
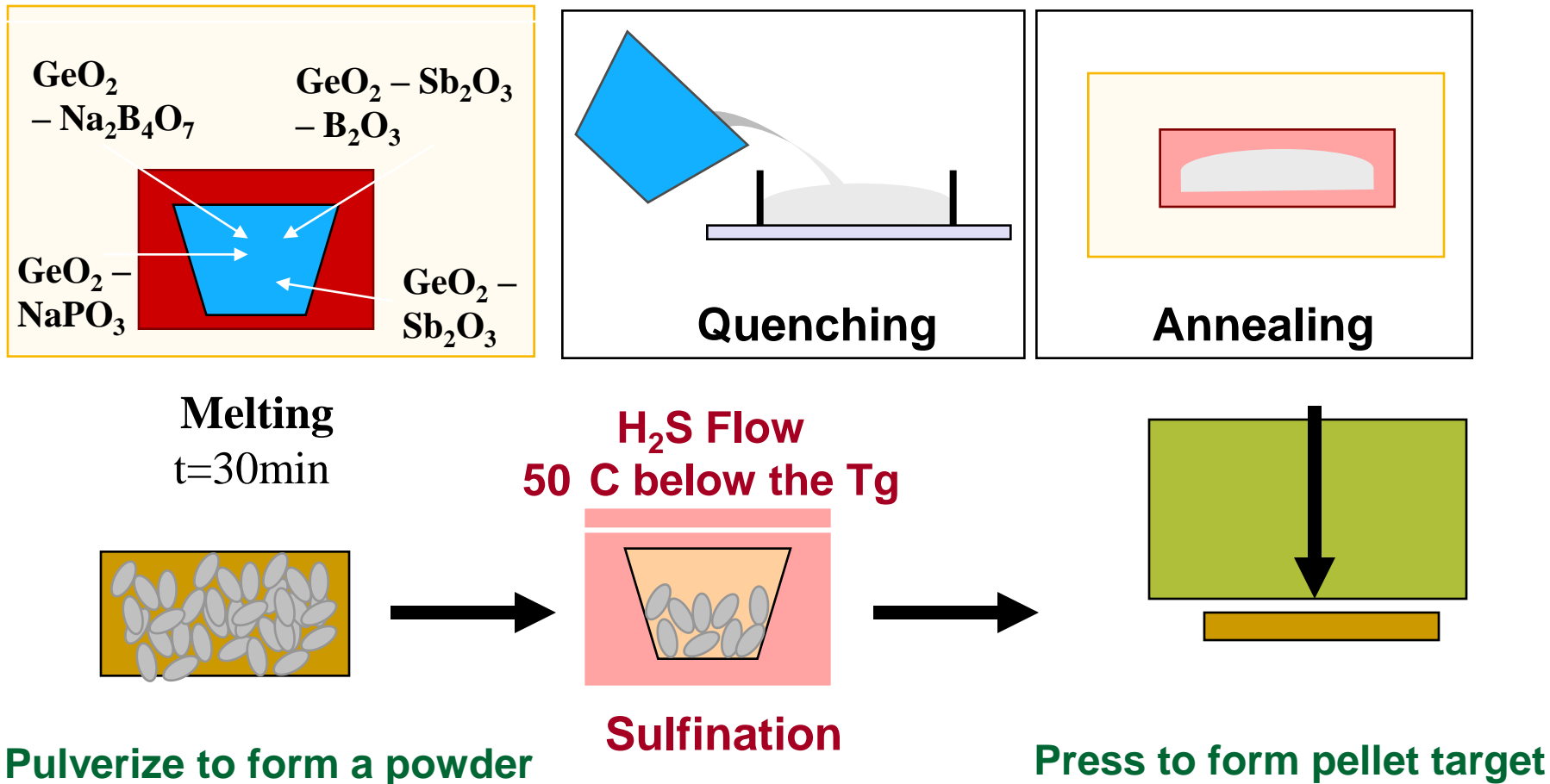
Sulfination process (*crystalline GeO$_2$*)

♦ **Raman spectrum** λ_{exc} = 632 nm

$\Rightarrow$ **Ge – O bond**

♦ **Raman spectrum** λ_{exc} = 632 nm

$\Rightarrow$ **Ge – S bond**
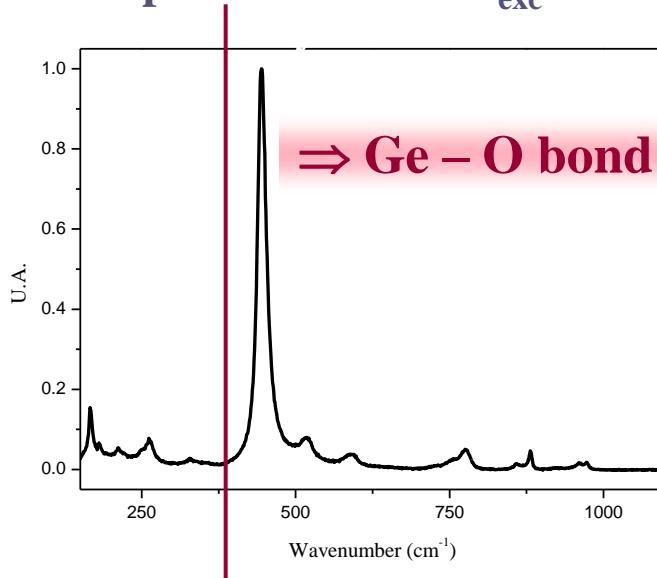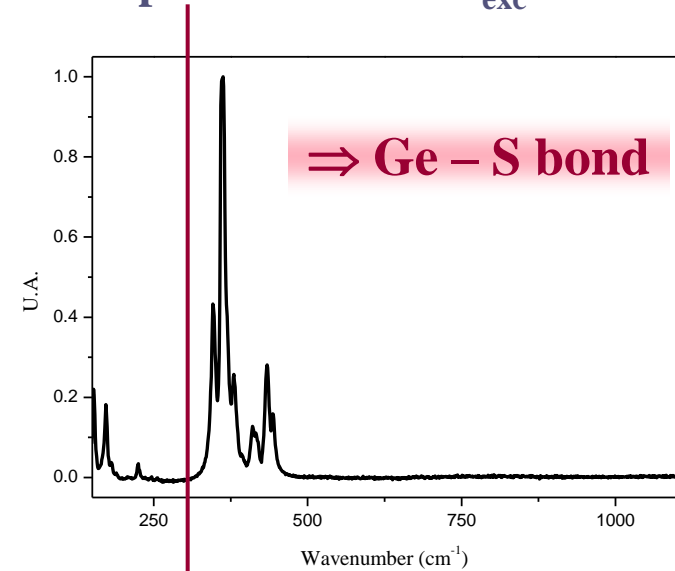
$\Rightarrow$ **Confirmation of substitution of oxygen by sulfur**

Confirmation of mixed oxysulfide

GeO_2 $\xrightarrow[\text{15 hours / 500 C}]{H_2S}$ $GeO_{1.6}S_{0.4}$

♦ **IR Spectra**

IR Forbidden mode of $[GeS_4]$

Asymmetrical stretch Ge – S – Ge in $[GeS_4]$

Asymmetric stretching $S_3Ge – GeS_3$
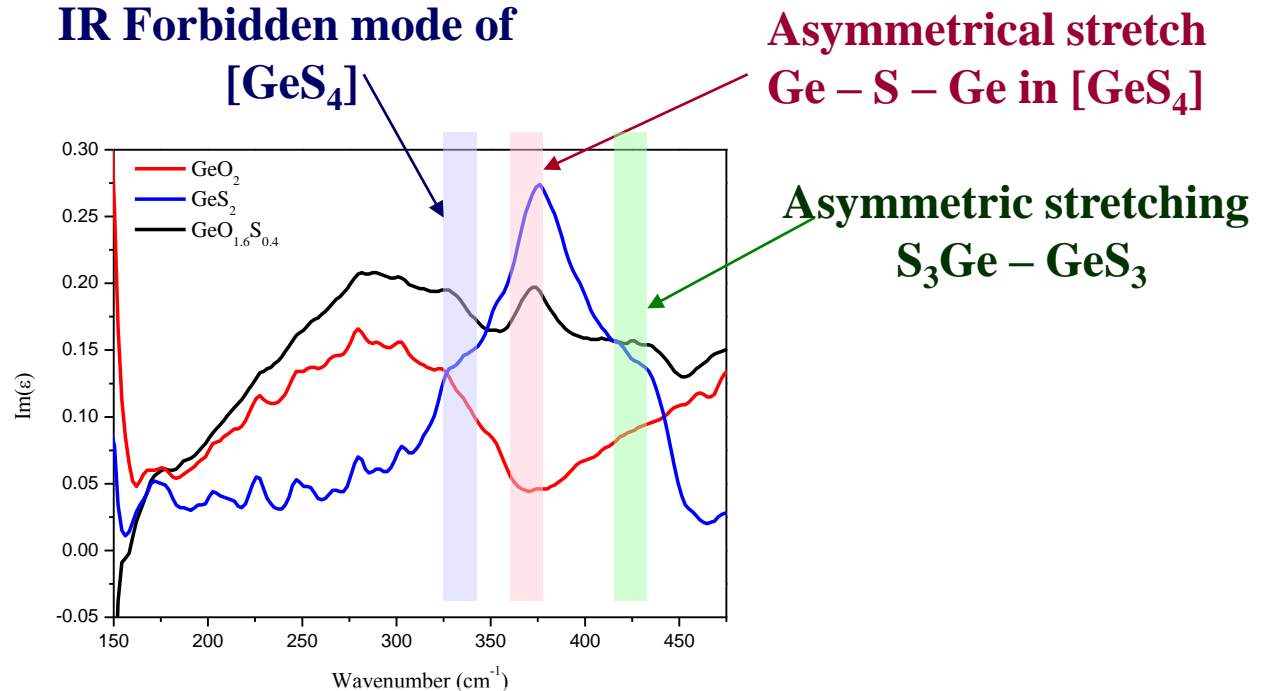
IR absorption peaks for $GeO_{1.6}S_{0.4}$ ⇒ Presence of Ge – S vibrations

Compositional tailoring of target

X-ray pattern of sulfinated GeO_2 powder
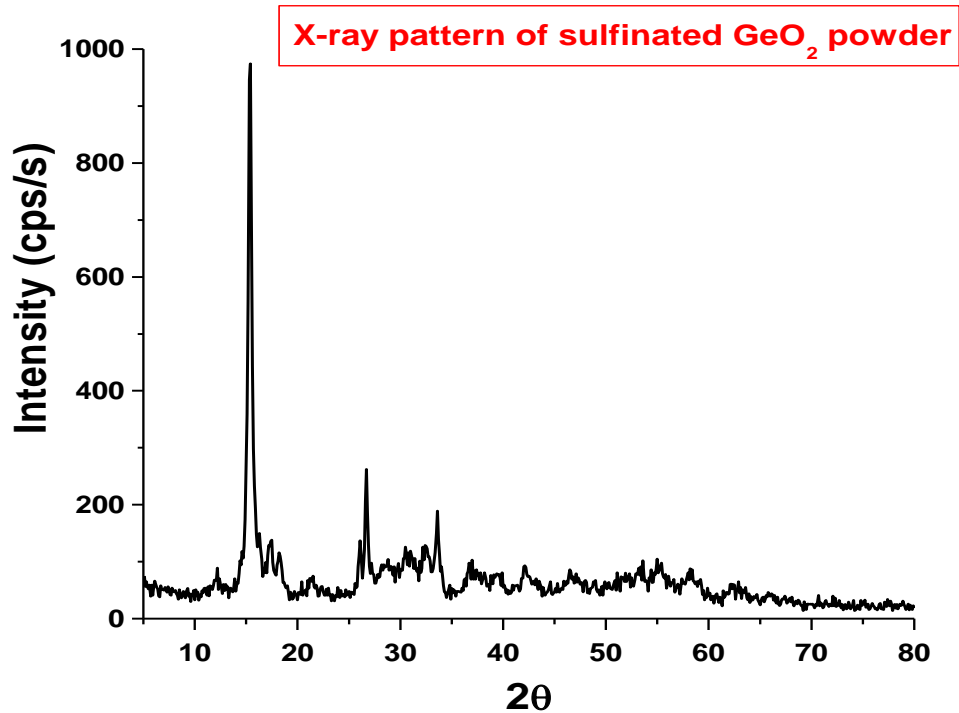
Composition	Sulfur percent
GeO_2	0
$GeO_{1.42}S_{0.58}$	29
$GeOS$	50
$GeO_{0.42}S_{1.58}$	79
GeS_2	100

Physical Vapor Deposition (aka RF sputtering)

Argon pressure of 10^{-2} mbar

Power applied of 15 mW

Homogeneous thin films obtained

High deposition speeds can be attained

Deposition speed of the material is correlated to O/S ratio of the target

No apparent selectivity of constituents in film

⟹ **Film thickness can be controlled**
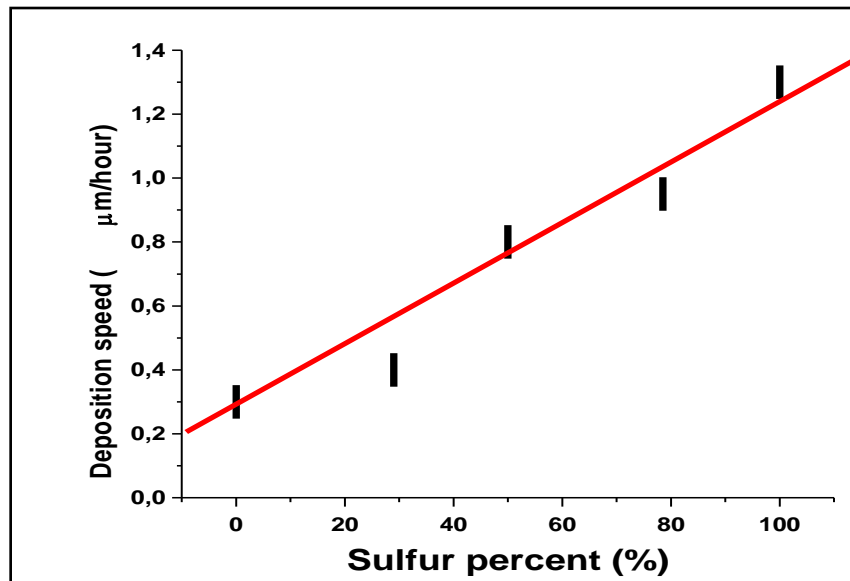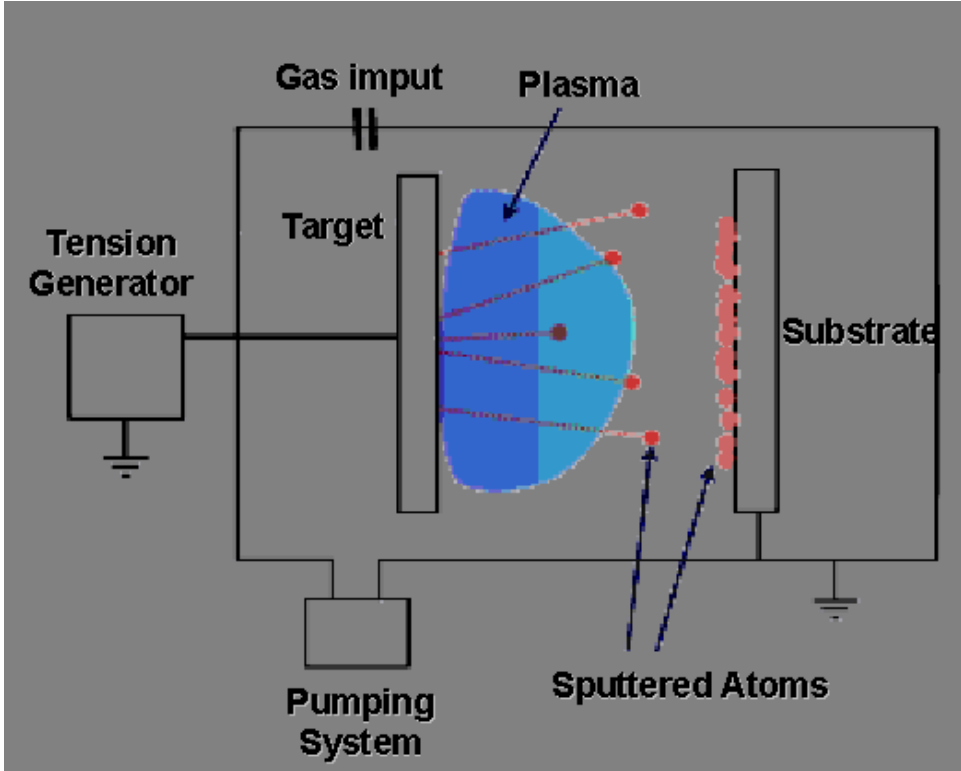
Oxide and oxy-sulfide films: morphology
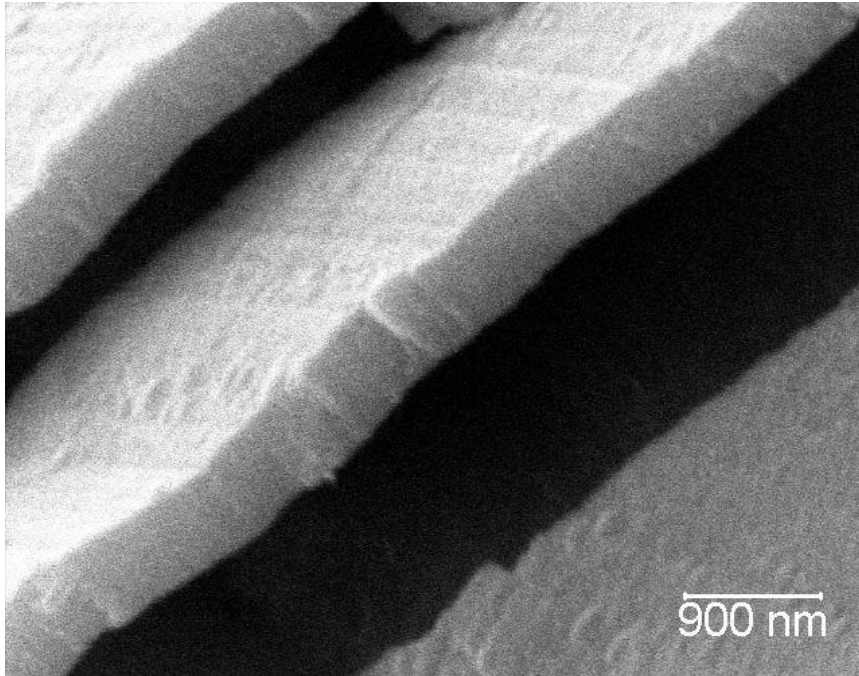
SEM image of GeO$_2$ thin film
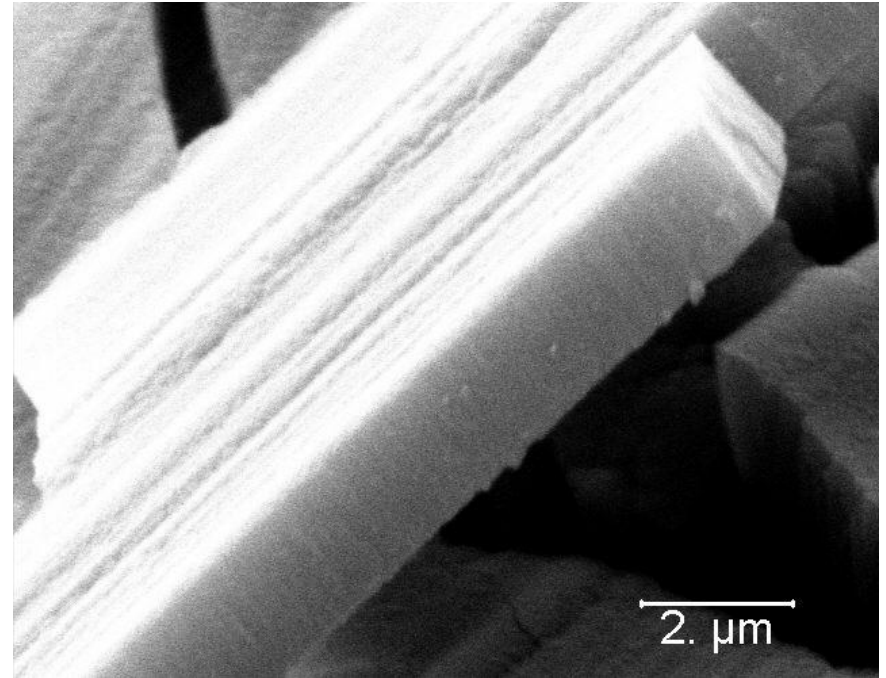
SEM image of GeO$_{1.42}$S$_{0.58}$ thin film

Auger data: compositional variation

Auger spectroscopy measurements

- Films deposited on Al foil

GeO$_2$

GeO$_{1.42}$S$_{0.58}$
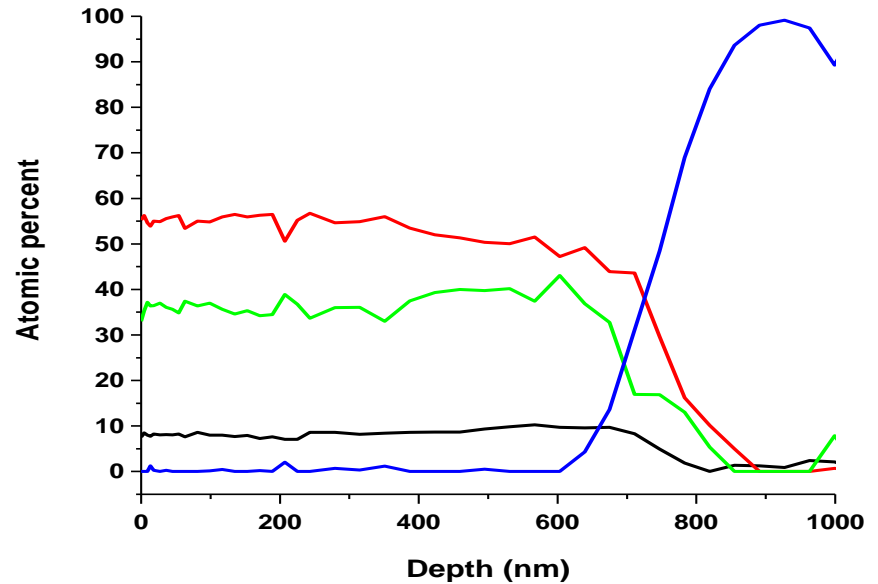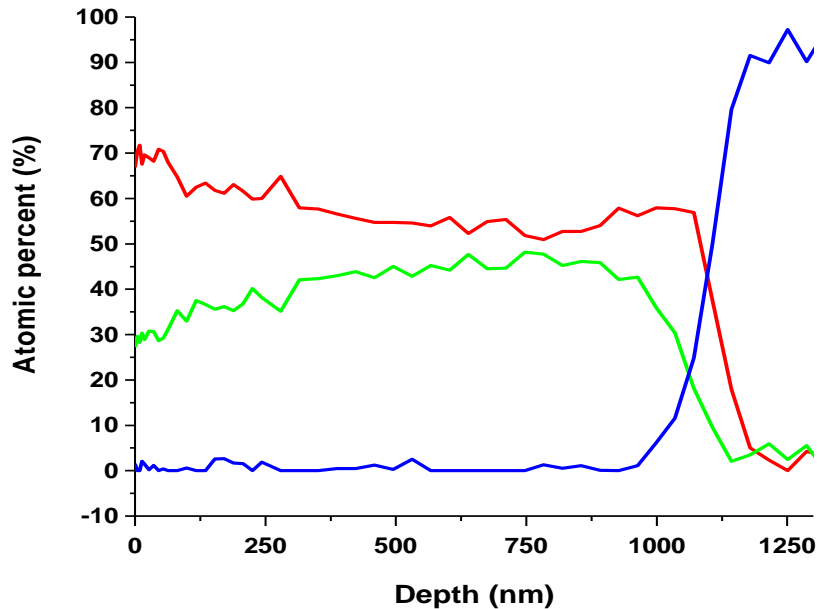
Homogeneity from the surface to the depth of the films

Legend:
- Aluminum (blue)
- Germanium (green)
- Sulfur (black)
- Oxygen (red)

Enhancement of optical and physical properties example: oxysulfide thin films

Absorption spectra

Legend:
- GeS$_2$ (red)
- GeO$_{0,42}$S$_{1,58}$ (black)
- GeOS (orange)
- GeO$_{1,42}$S$_{0,58}$ (magenta)
- GeO$_2$ (blue)

Y-axis: α (cm^{-1}), values: 0, 2500, 5000, 7500, 10000, 12500, 15000, 17500

X-axis: wavelength (nm), values: 300, 400, 500, 600, 700, 800
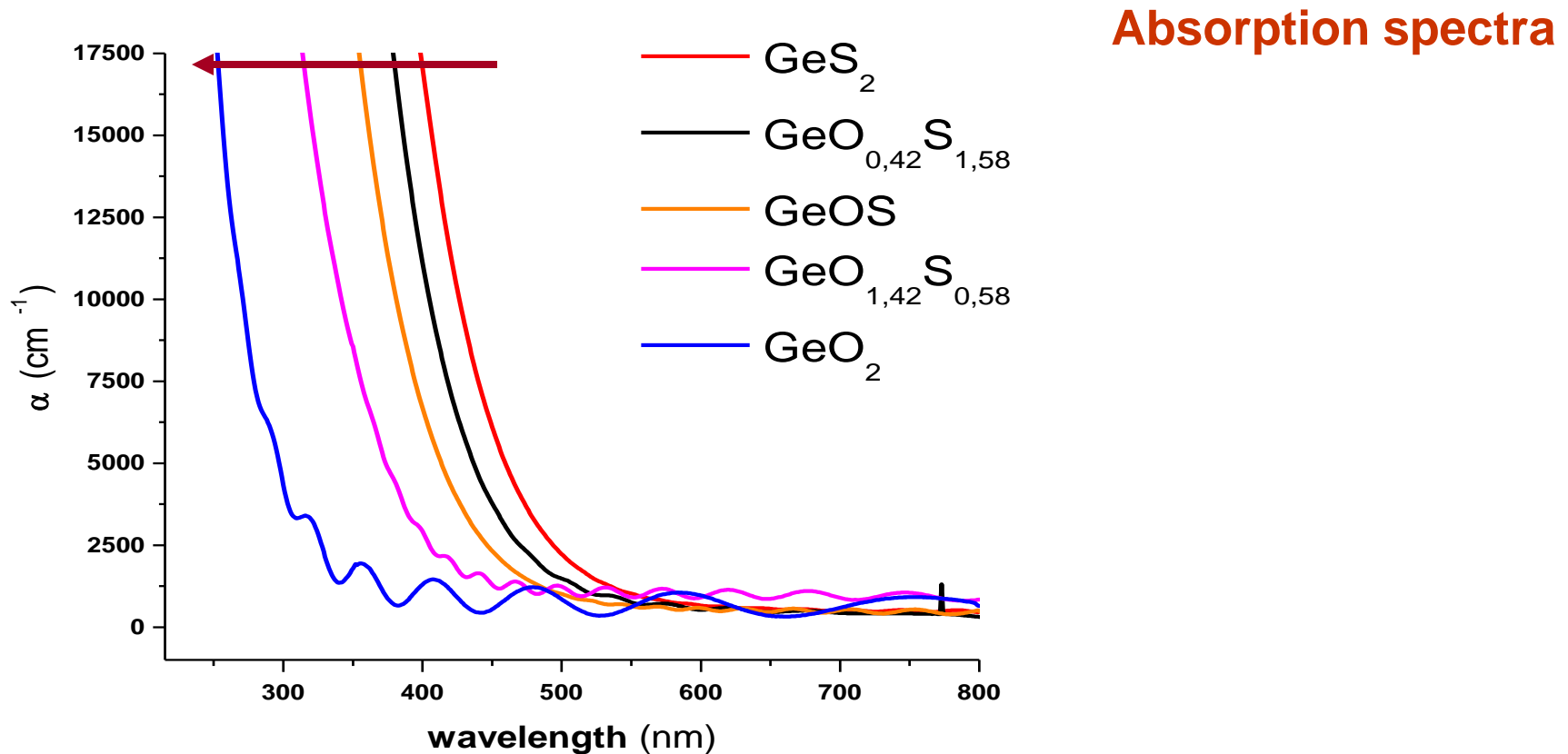
Blue-shift with decreasing sulfur content (UV and multiphonon); increased T_g, thermal stability and mechanical integrity of resulting film material

Structure of Glass: Section being lectured

Micro-Raman spectroscopy: structural origin of changes

GeO$_4$ associated vibrations

Nomalized micro-Raman spectra at 514 nm

Ge-Ge

Wavenumber (cm^{-1})

Nomalized Intensity

Legend:
- GeS$_2$
- GeO$_{0,42}$S$_{1,58}$
- GeOS
- GeO$_{1,42}$S$_{0,58}$
- GeO$_2$
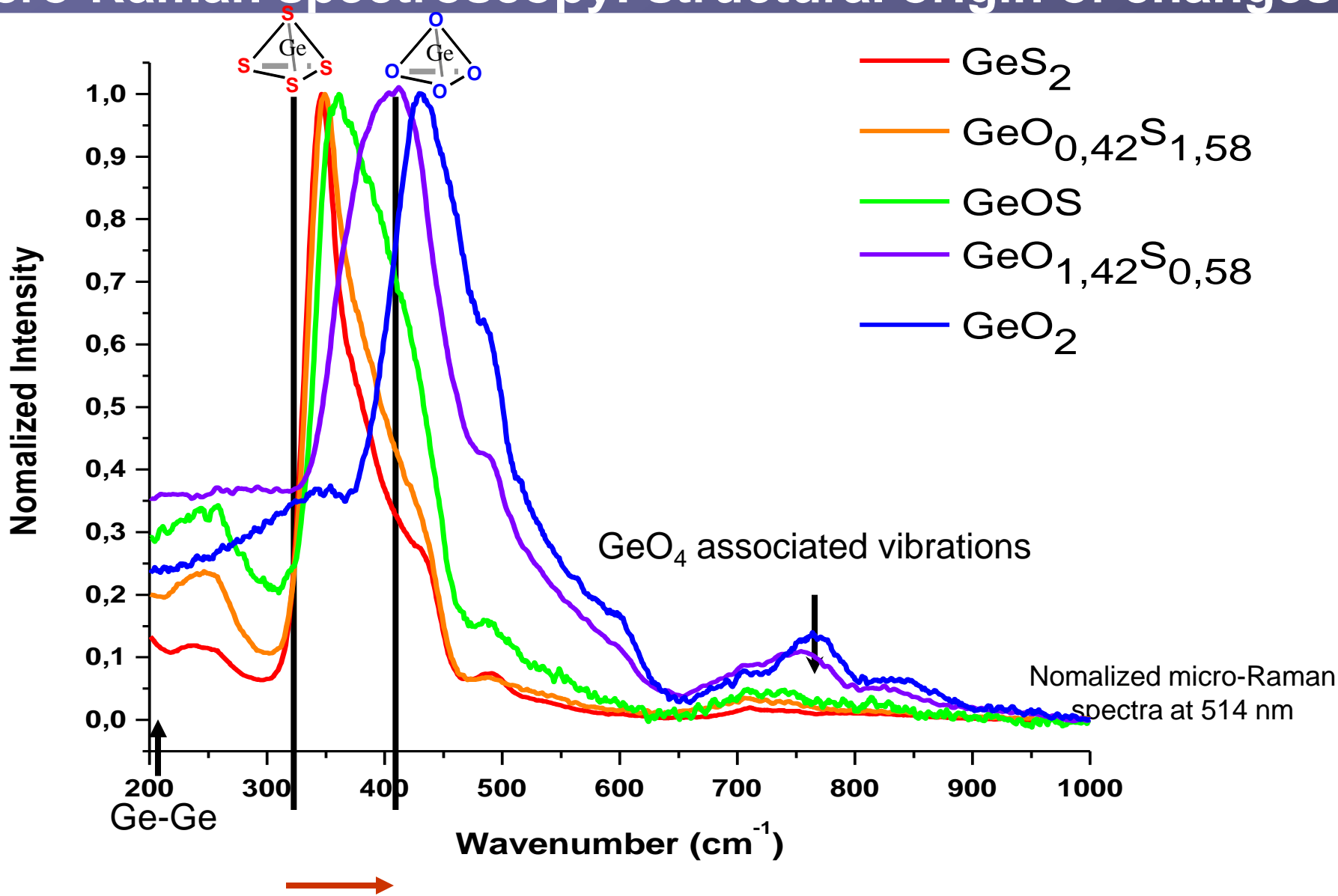
Vibration of tetrahedral unit peak shifts with sulfide to oxide ratio

Y. Kim, J. Saienga, S. W. Martin, J. Non-Cryst Solids, 351 (2005), 1973-1979

Other applications driving film processing technology: *Portable Energy Sources are Critical Technologies*

Anode and Cathode Combinations Determine the Energy Density
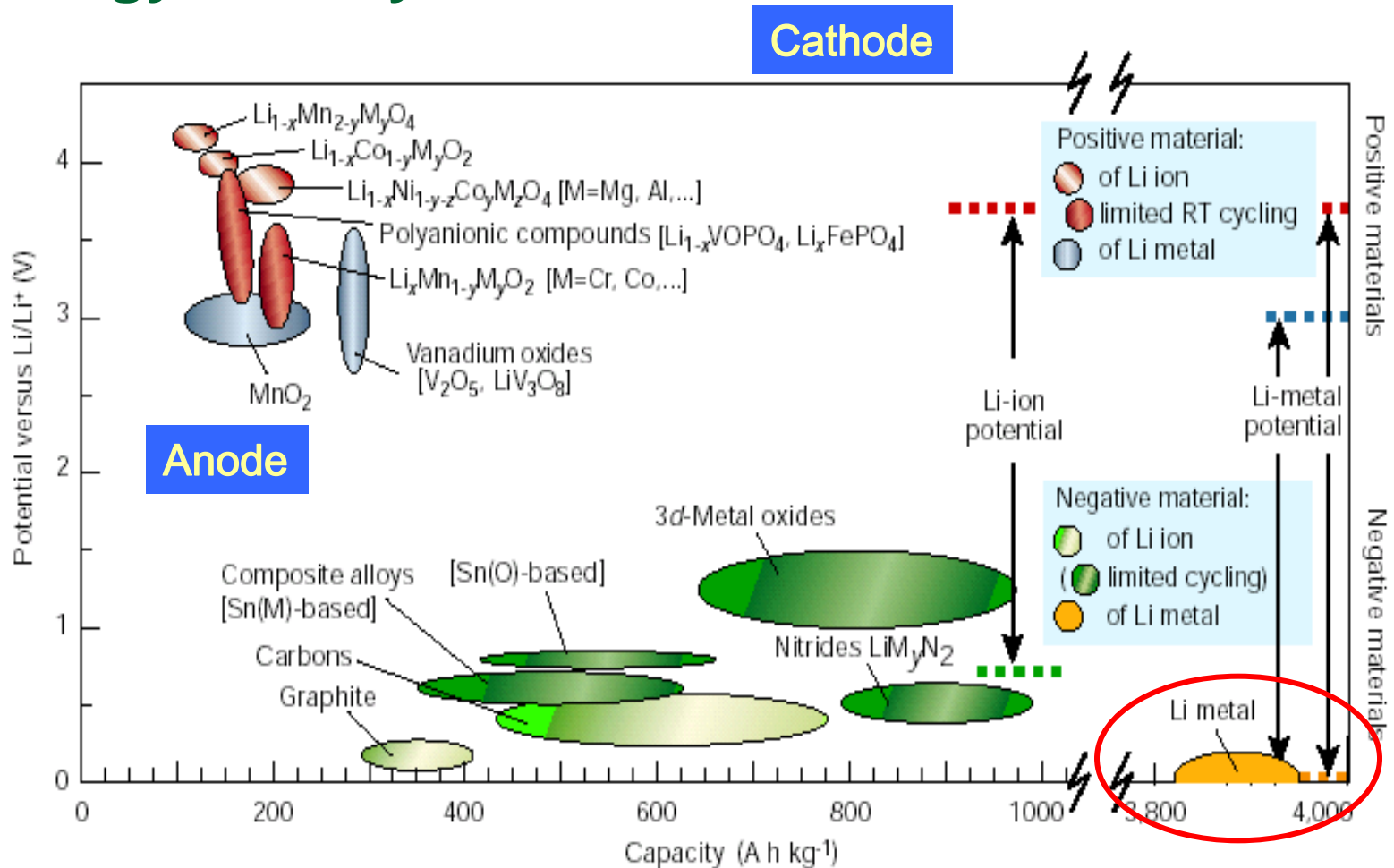
J.M. Tarascon, M. Armand, Nature, 414, 15 (2001) 359

Li-ion Batteries

C_6 is a common anode material for Li-ion batteries

The maximum capacity of graphite (LiC_6): 372 mAh/g 1339 C/g

Good cycle-life

But, low capacity for new portable devices
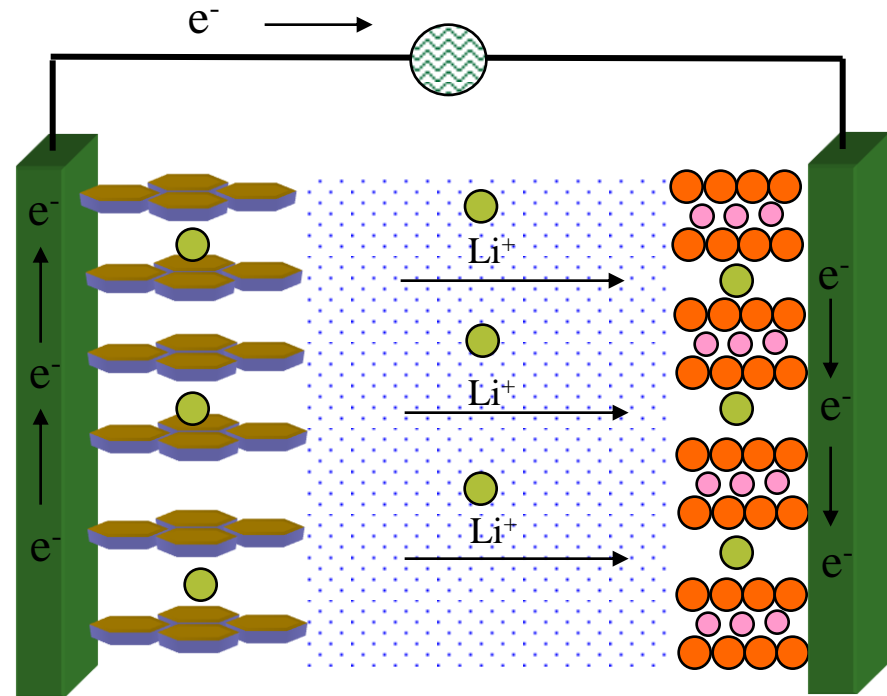
Li_xC_6 Li^+ conducting electrolyte $Li_{1-x}CoO_2$

Anode: $Li_xC_6 \longrightarrow xLi^+ + xe^- + C_6$

Cathode: $Li_{1-x}CoO_2 + xLi^+ + xe^- \longrightarrow LiCoO_2$
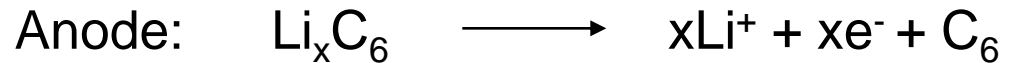
Polymer Li⁺- ion Conducting Electrolytes

- **Li ion conducting polymer electrolytes**
  - *Advantages*
  - Polypropylene oxide + $LiClO_4$ (Salt + polymer electrolyte)
  - High Li^+ ion conductivity
  - Excellent thin film properties
  - Enable multitude of "form factors" for use

  - *Disadvantages*
  - Chemically unstable
  - Degrades with time
  - Soft
  - Cannot be used high energy anodes such as Li

Lithium Dendrite Formation in Li ion Batteries with polymer electrolyte membranes
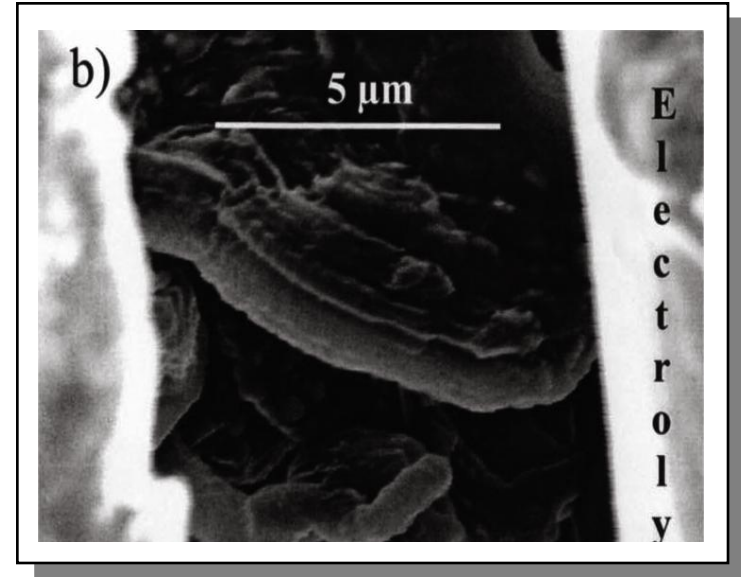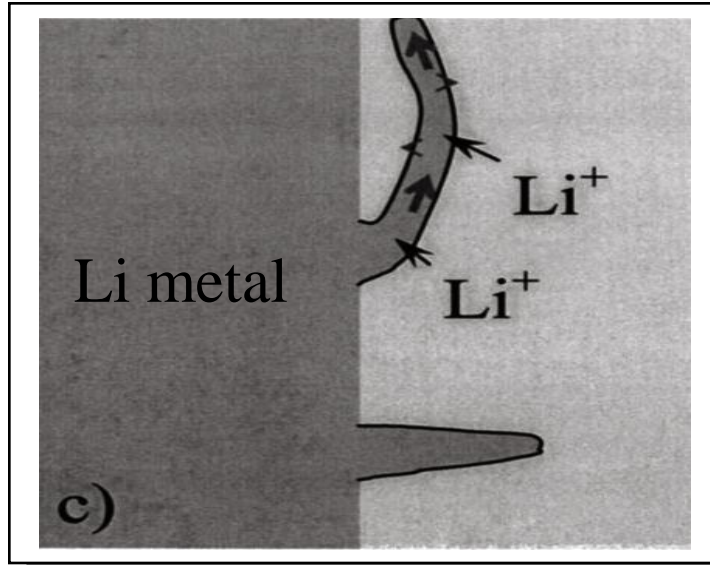
Non-epitaxial deposition of lithium after each cycle leads to the growth of uneven "fingers" or dendrites

Internal connection results which short circuits the battery

M. Dolle et al. Electrochemical and Solid-State Letters, 5(12) (2002)A286

Li$^+$ - ion Conducting Glasses (FIC) as Alternative Electrolytes

- ***<u>Advantages</u>***
- Inorganic chemistry can be more chemically stable
  - No reaction with high activity anodes
- Stronger bonding (ionic) gives higher mechanical strength
  - No Li penetration from dendrites
- Chemically bonded anion (Si-O$^-$, Ge-S$^-$) is immobile
  - Unit transference number for Li$^+$
  - Higher Li$^+$ ion conductivity
- Smaller temperature dependence of the conductivity
  - Polymers are used above Tg in liquid state
  - Glasses are used below Tg in solid state

Li⁺- ion Conducting Glasses as Alternative Electrolytes

- ***<u>Disadvantages</u>***
- Solid structure does not accommodate volume changes
- Anode and cathode shrink and swell during discharge
- Anode and cathode swell and shrink during recharge cycle
- Volume changes promote debonding between electrode and electrolyte
- Debonding creates open circuit and reduces battery performance

Thio-Oxynitride FIC Thin Films

A

E

C

- Combine electrochemically durable inorganic electrolyte with flexible and volume accommodating polymer electrolyte
    - Thin strong Li^+ ion conducting film will block dendrite growth
    - Polymer electrolyte will allow required volume changes in the battery
- Oxide chemistry to enable atmospheric stability for ease of handling
- Sulfide chemistry to enable fast Li^+ ion conduction and transport across thin film electrolyte
- Nitride chemistry to enable electrochemical stability in contact with metallic Lithium

Thio-Oxynitride FIC Thin Films

- ***Solution***
  - Back Lithium metal anode with copper current collector on back side
  - Coat Lithium metal anode with inorganic glass FIC electrolyte on front side
  - Sandwich the two layers together to create new stable anode
  - Copper protects backside and collects electrons
  - Inorganic glass protects front side – carries Li^+ ions to polymer electrolyte
  - Strippable polymer film is removed when battery is manufactured
  - Thin glass film
    - Limits dendrites, hard inorganic glass
    - Protects polymer electrolyte from reactive Lithium

A

E

C

Copper

Lithium

FIC Glass Film

Strippable plastic
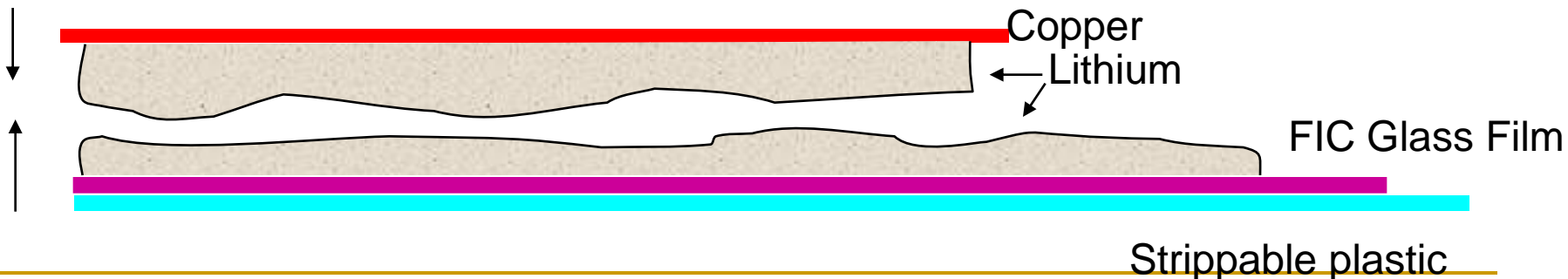
Thio-Oxynitride FIC Thin Films

- ## Problems with existing glasses
  - Glass compositions that are stable in contact with metallic Li are not conductive enough to Li^+ ions
    - Oxide Glasses
    - $Li_2O + P_2O_5$
  - Glasses that have high enough Li^+ ion conductivities are not stable enough in contact with Li
    - Chalcogenide Glasses
    - $Li_2S + GeS_2$
- ## Solutions
  - Can oxy-sulfide mixtures be both conductive enough and stable enough?

Thio-Oxynitride FIC Thin Films

- Bates at Oak Ridge also found that nitrogen added to oxide glasses makes them stable in contact with Li
  - Li_3PO_4 + N (RF reactive sputtering) produces $Li_{3.3}PO_{3.9}N_{0.17}$
  - Good stability with Li
  - But poor conductivity 10^{-6} $(\Omega cm)^{-1}$ at RT
- Sulfides can be sputtered in Ar and have excellent conductivities, but poor stabilities
- Will Thio-Oxynitride thin films combine properties of all three components?

Thio-Oxynitride RF sputtered thin films

- Objectives of the ISU project
  - Build RF magnetron reactive materials sputtering system capable of sputtering chalcogenide targets
  - Test with Li_3PO_4 in Ar and N
    - Characterize Li_3PO_4 and LiPON
  - Sputter Chalcogenide Targets, Li_4GeS_4
    - Sputter in Ar and N
    - Oxygen as a ubiquitous contaminate used to advantage
    - Characterize structure, properties, conductivities
    - Improved atmospheric stability?
    - Improved stability with Li metal?
    - Improved conductivity?

Thionitride Thin Films – ISU effort

- 2004-2005
- Construction of RF magnetron sputtering system
  - Attached to a N_2 filled glove box
  - Tested and debugged sputtering system, glove box, and vacuum system
- Purchased commercial Li_3PO_4 target
  - Sputtered Li_3PO_4 target in Ar – No N incorporation
  - Sputtered LI_3PO_4 target in N_2 – N incorporation
    - ~ the same amount of N reported in literature
    - ~ the same atomic ratios of Li, P, and O
  - Achieved ~ 1μm/hr deposition rate
  - Controllable sputtering gases, power, time, and pressure
  - Connected to glove box so targets and deposited films can be handled without contamination

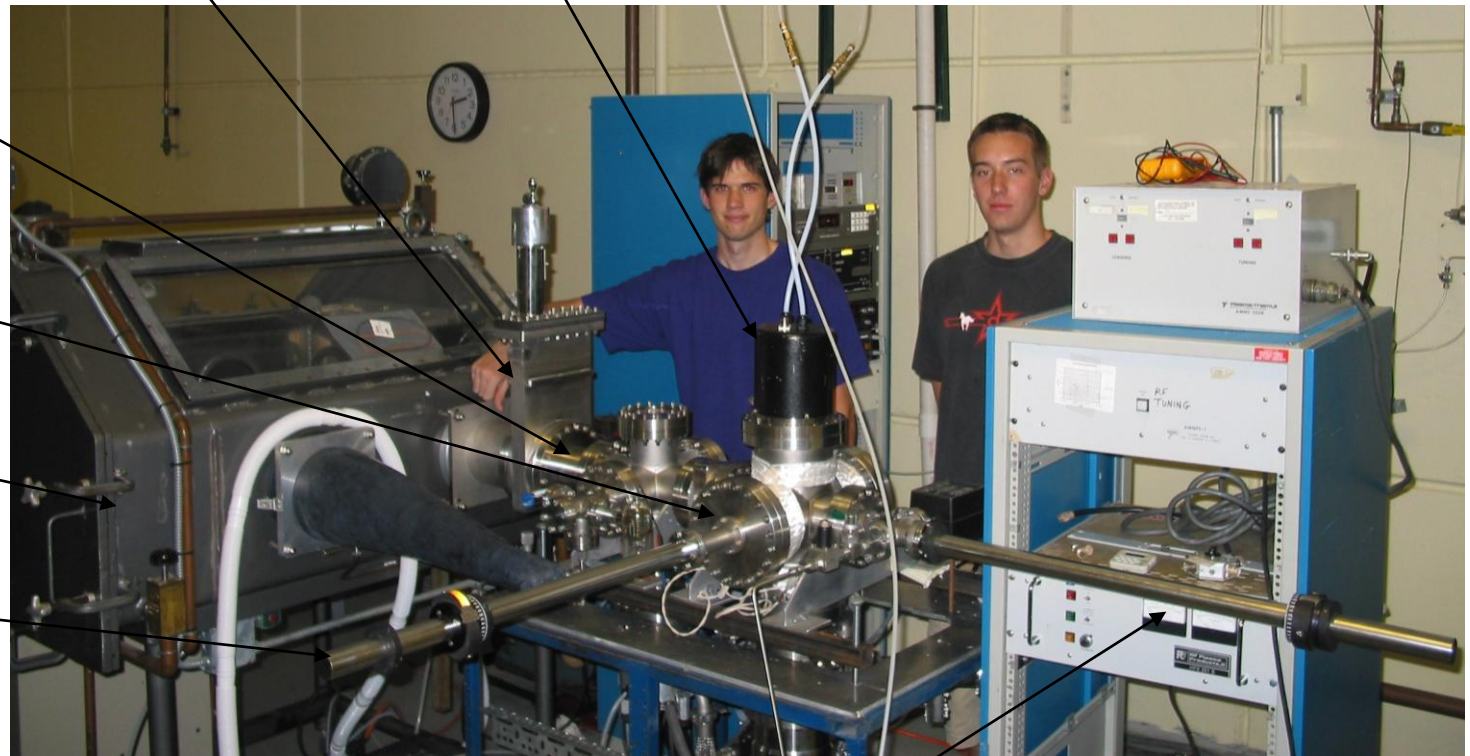# Reactive Materials RF Sputtering System

Load lock chamber

Sputtering Head

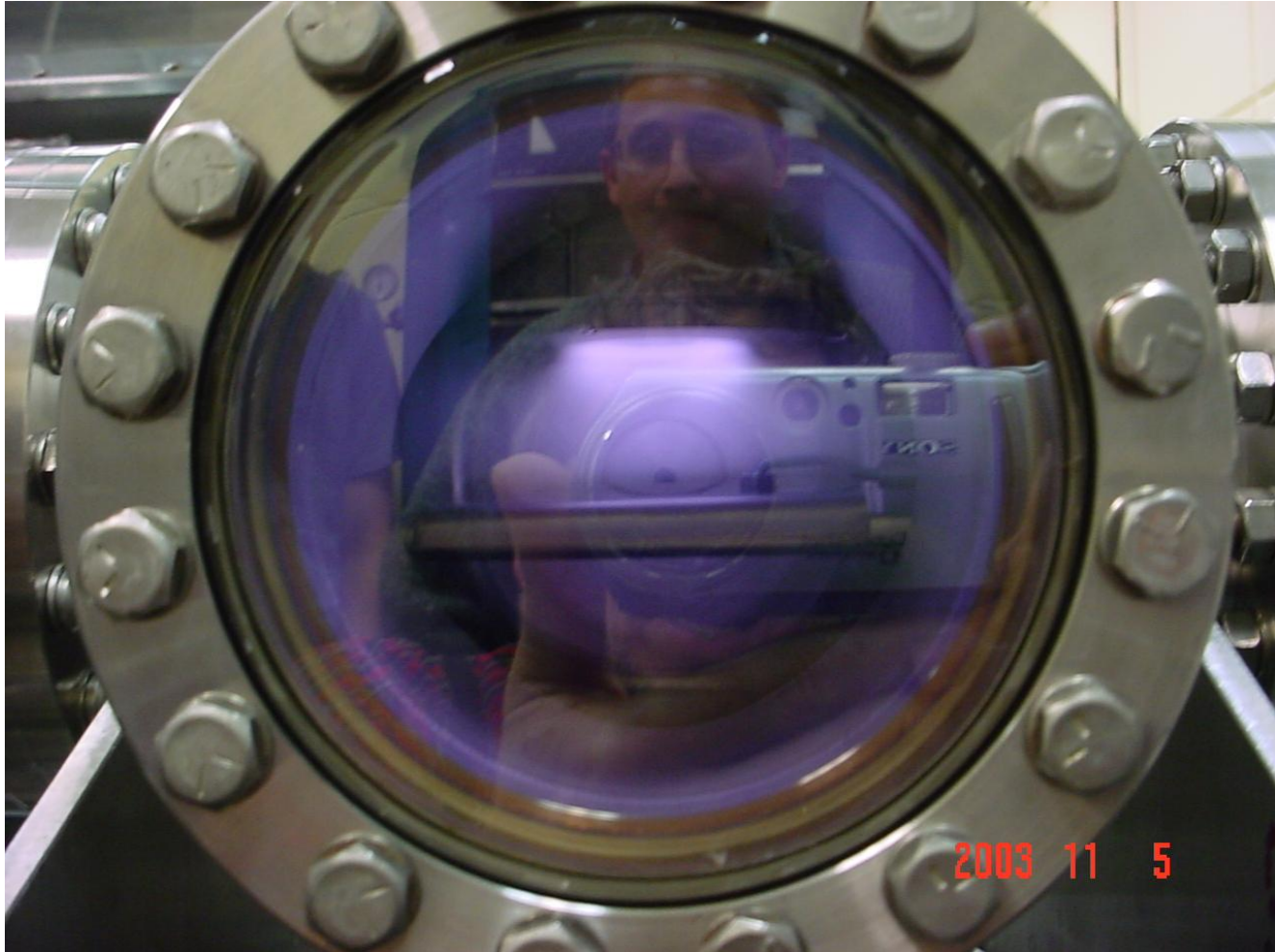Sputtering anti-chamber

Sputtering Chamber

Glove box

x load lock arm

y load lock arm

# Li$_4$GeS$_4$ plasma in N$_2$ at ~ 20 mTorr

Li$_4$GeS$_4$ Target Preparation

- Commercial source for Li$_2$S – Lorad, Alfa, Cerac
- Ge + 2S → GeS$_2$ – Sealed SiO$_2$ tube, 800 ^{o}C for 8 hours with rotation @ 5-8 rpm
- 2Li$_2$S + GeS$_2$ → Li$_4$GeS$_4$, 900°C for 2 hours
  - Vitreous carbon crucibles
  - Slowing cooling to ensure crystallization of the melt
  - Milling of the powder to ~ 5-25 microns
- Dry pressing to a 1/8" x 2" pellet
- Sintering 700, 720, 740, 800 ^{o}C, 2 – 6 hours

Sample preparation facilities at ISU

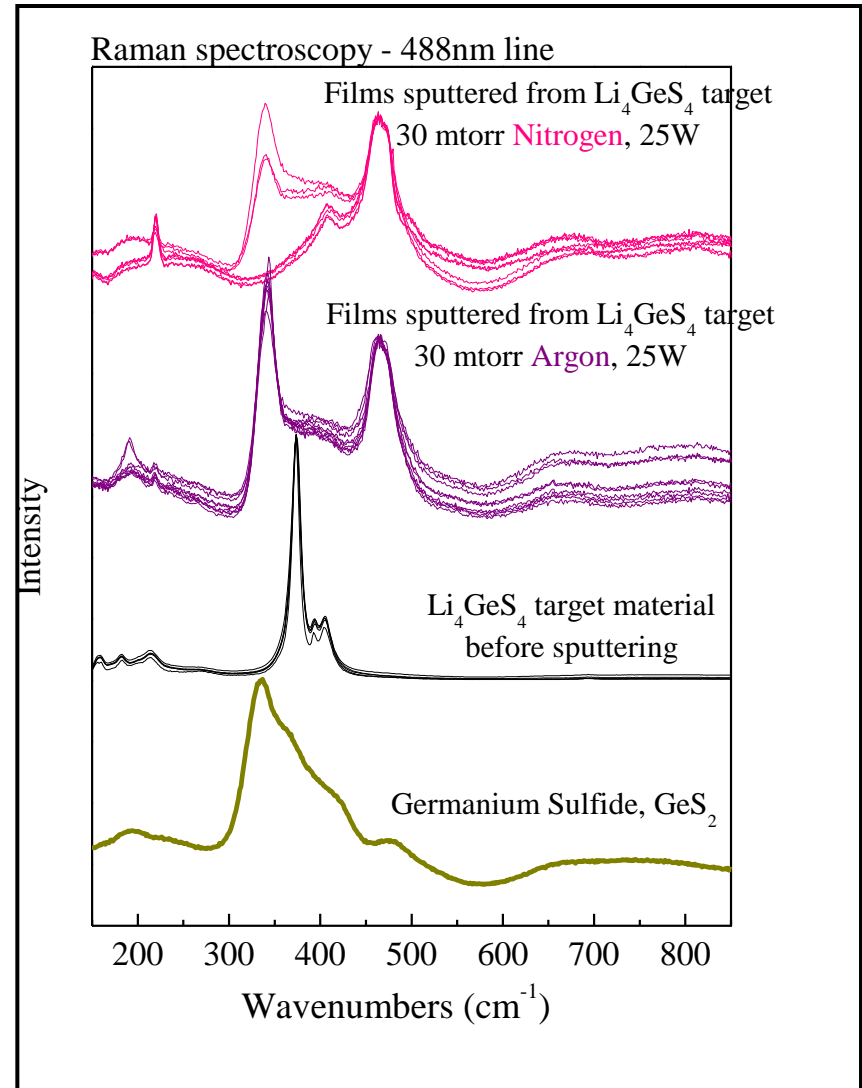# Li$_4$GeS$_4$ Target Characterization - XRD
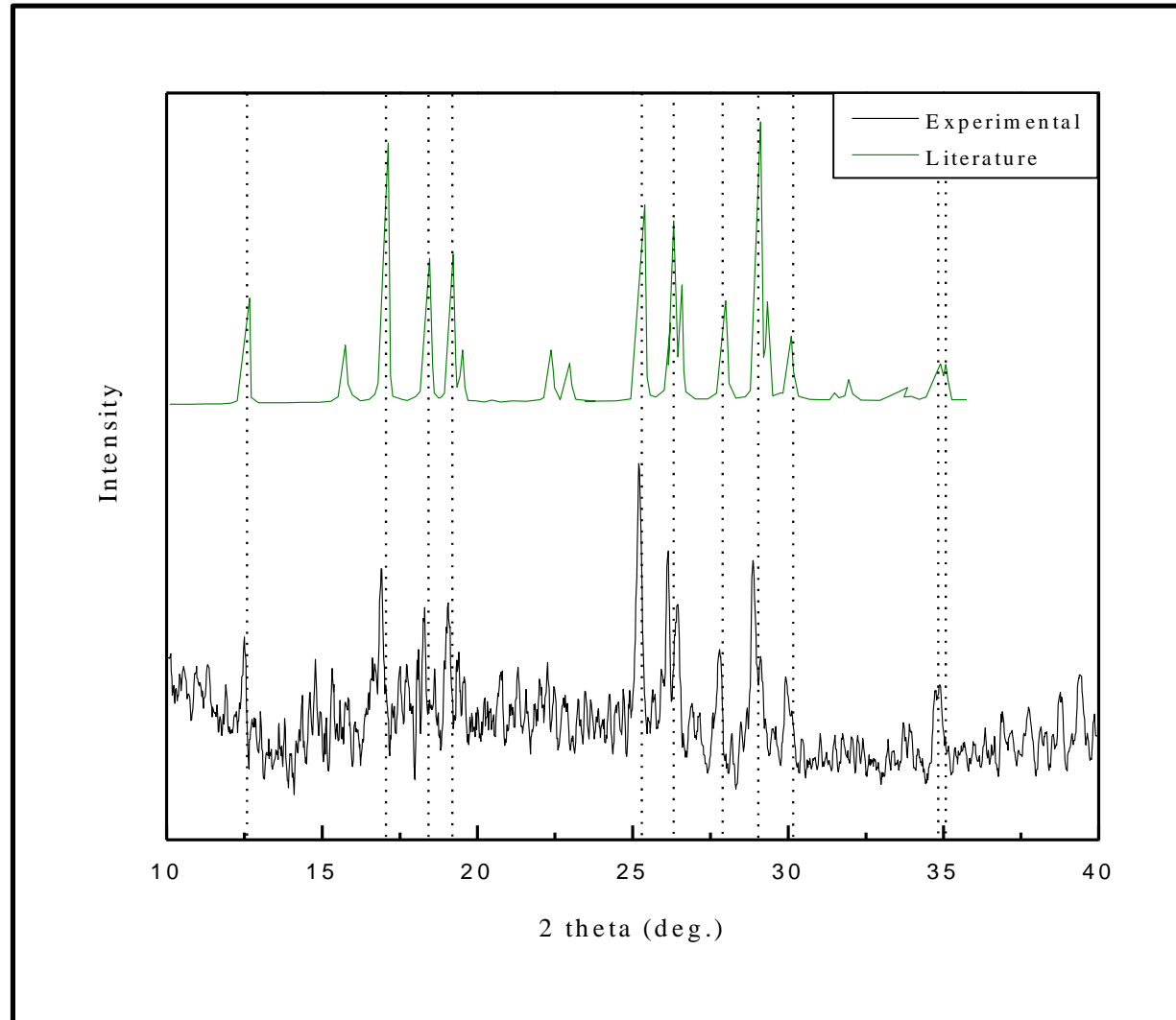
Li$_4$GeS$_4$ Target Characterization

- **Effects of Sintering Time and Temperatures**
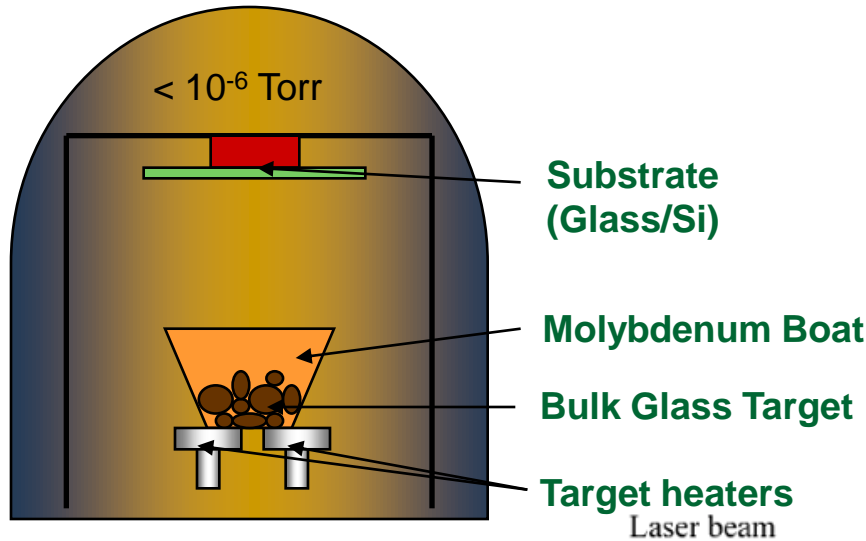 - Green bulk density 1.91 g/ml
  - Theoretical density 2.25 g/ml

Time	Temp (C)	Apparent Density (g/ml)
2 hrs	730	2.052
	740	2.173
	750	2.203
4 hrs	740	2.147
	750	2.399

Sputtering of Li_4GeS_4 thin films

- Raman Spectra
- Li_4GeS_4 shows sharp lines from GeS_4^{4-} tetrahedra
- Sputtered films in N_2 and Ar are very similar
- Shows evidence of bridging sulfur units
- Under modified with Li
- GeS_2 is more easily sputtered than Li_2S

Raman spectroscopy - 488nm line
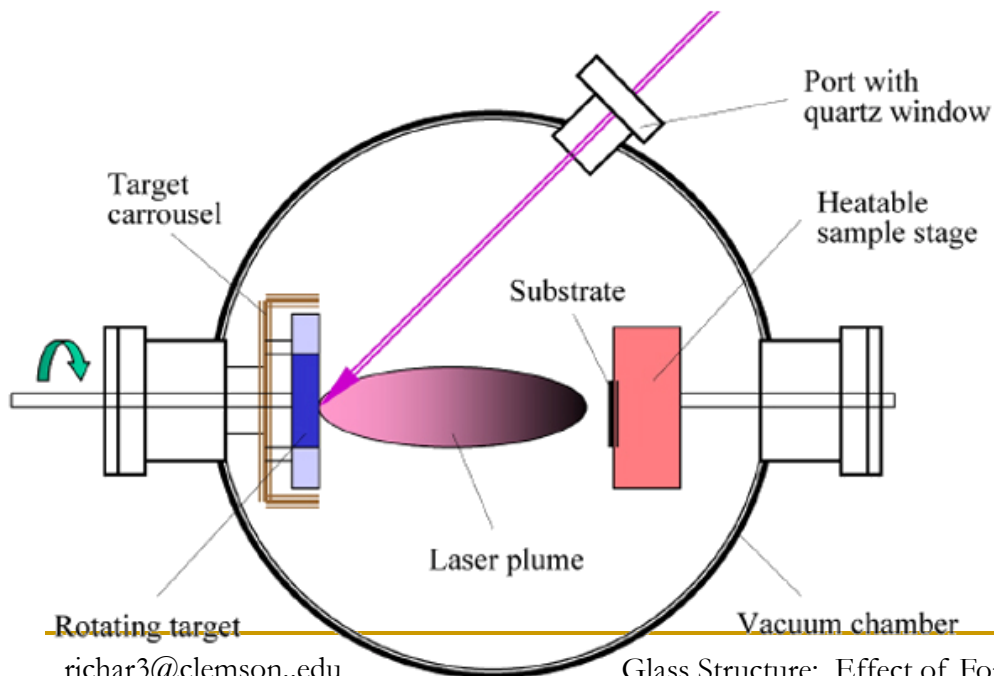
Films sputtered from Li_4GeS_4 target 30 mtorr Nitrogen, 25W

Films sputtered from Li_4GeS_4 target 30 mtorr Argon, 25W

Li_4GeS_4 target material before sputtering

Germanium Sulfide, GeS_2

Intensity

Wavenumbers (cm^{-1})

Film Deposition Techniques

< 10⁻⁶ Torr

Substrate (Glass/Si)

Molybdenum Boat

Bulk Glass Target

Target heaters

Thermal Evaporation

Deposition parameters:
112 Evap-Sputter Station (PVD Systems Inc)
Thermostat stage held to 25 C
Base pressure: 2.0×10^{-7} Torr
Deposition rate: ~2 nm/s

Laser beam

Port with quartz window

Target carrousel

Heatable sample stage

Substrate

Laser plume

Rotating target

Vacuum chamber

Pulsed Laser Deposition

Laser parameters:
Mode-locked Nd:YVO$_4$ laser
Frequency tripled – 355 nm
Repetition rate: 28 MHz
Pulse width: 12 ps
Peak intensity: ~10^{10} W/cm^2

Deposition parameters:
Target-Substrate distance: 160 mm
Base pressure: 5.0×10^{-7} Torr
Ablated using 2.5 cm spiral pattern

Characterization tools - films

- Composition and thickness – **SEM w/EDS**
- Refractive Index, thickness and extinction coefficient - **Ellipsometry**
- Refractive Index change (Δn) -
  - Stress birefringence measurements (magnitude and sign of stress)
  - Induced refractive index change
- Thermal properties (μTMA, thermal conductivity) - **Micro-thermal analysis**
- Bonding and local structure/structural changes - **Micro-Raman and Waveguide Raman Spectroscopy (WRS)**
- Composition/stoichiometry, thickness, density - **Rutherford Backscattering Spectroscopy (RBS)**

Lecture 23 Ends here

Scanning Electron Microscopy (SEM) with Energy Dispersive Spectroscopy (EDS)
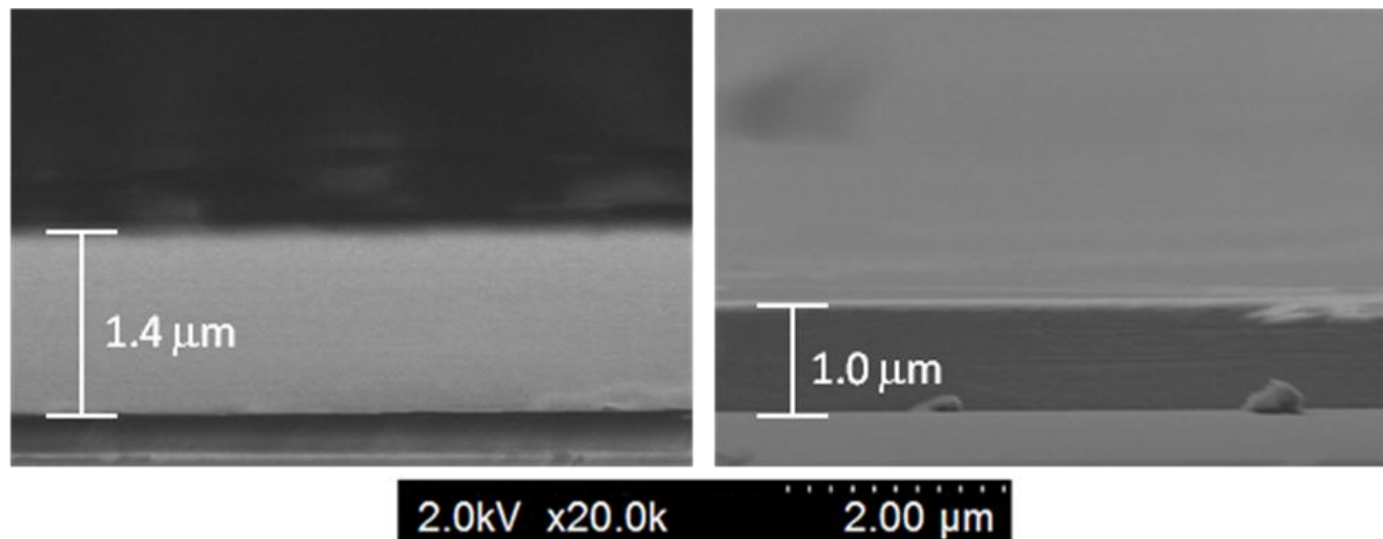

Deposition Method	Target	Thickness	% Ge	% Sb	% S
Thermal	$Ge_{0.23}Sb_{0.07}S_{0.70}$	1400 nm	23	11	66
PLD	$Ge_{0.23}Sb_{0.07}S_{0.70}$	1000 nm	23	7	70

- **PLD film appears to have a composition closer to that of the bulk target**
- **Difference is close to limit of error for the measurement (2 at.%)**
- **Both films appear to have homogenous structure through the thickness**

BASIC OPTICS

Θ_1 Θ_1

refractive index n1

reflected

refractive index n2

Θ_2

refracted
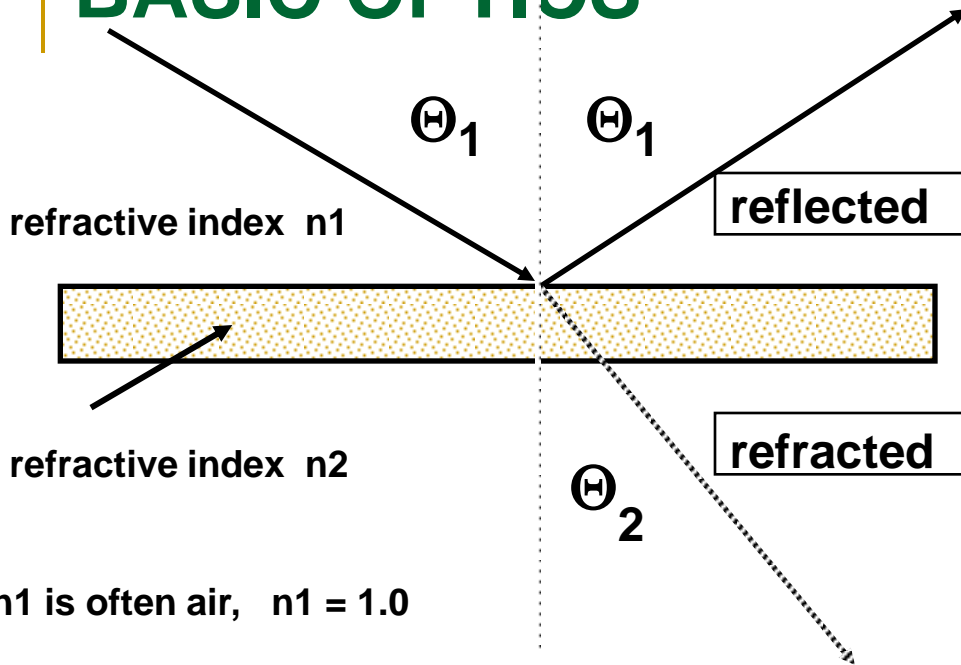
*n1 is often air,   n1 = 1.0

$$r = \left[\frac{n1 - n2}{n1 + n2} \right]^2$$

**Fresnel
single surface
reflection, r**

Helpful relationships

(1) $c = c_o/n$ where:

  c_o = speed of light in vacuum
  n = refractive index of medium
  c = speed of light in medium of refractive index n

(2) heavier atoms (higher Z) with *more* polarizable electrons can be influenced
(rearranged by an E-field); these materials have a higher n
      [i.e. S, Se have n>2; Si, Ge have n between 3 and 4]

(3) index *tends to* track with density $\uparrow \rho$ -------> $\uparrow$ n

index measurement: Swanepoel Method

The transmission of a substrate material alone is given by the well-known formula

$$T_s = \frac{(1-R)^2}{1-R^2} \qquad \text{with} \qquad R = \left[(s-1)\big/(s+1)\right]^2$$

Where s is the refractive index of the substrate. For a thin film deposited on a substrate, interference fringes occur for:

$$2nd = m\lambda$$

In the transparent region of the spectrum, Swanepoel showed that the envelope function of the maxima is the same as the substrate and the minima are given by:
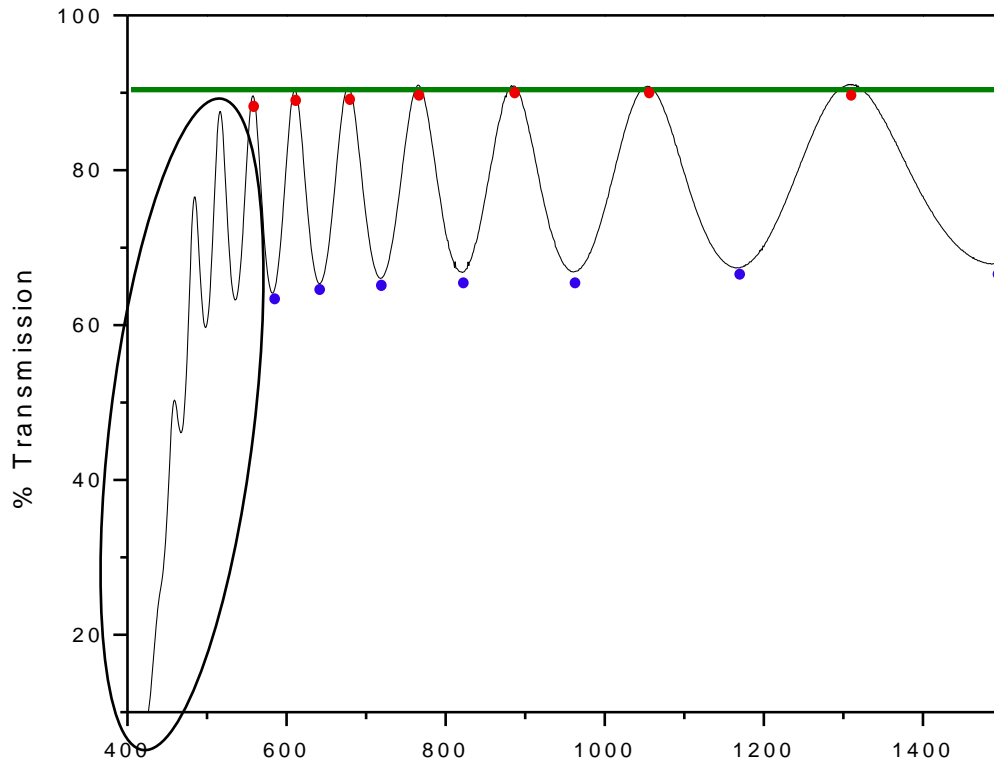
$$T_m = \frac{4\,n^2 s}{n^4 + n^2\left(s^2+1\right) + s^2}$$

Transmission spectra before and after irradiation
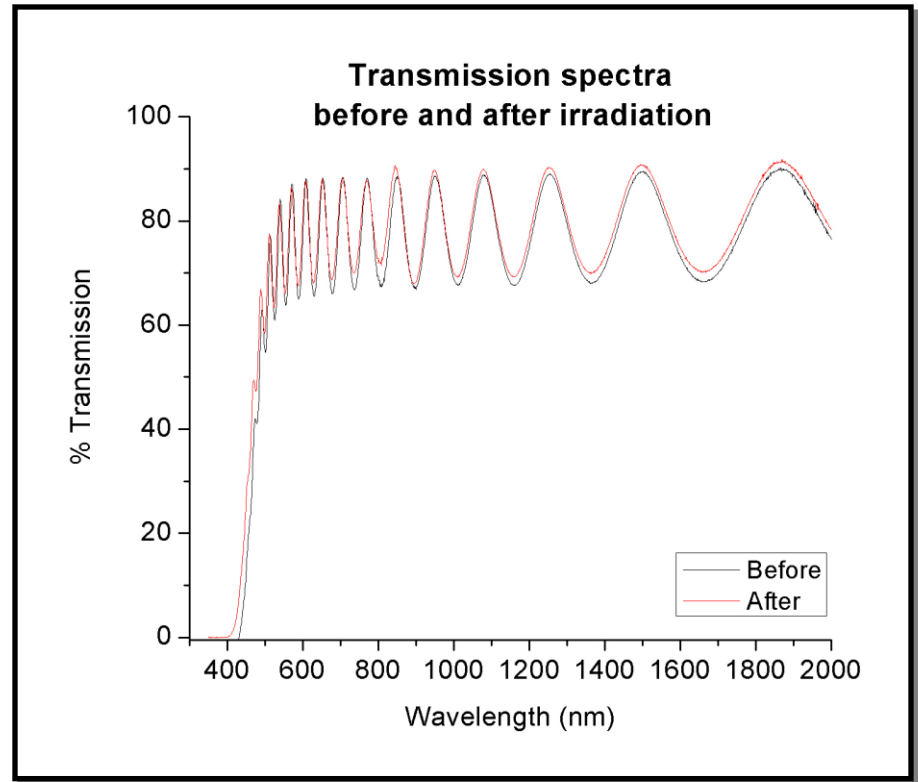
Thus, we can solve for n by:

$$n = \left[M + \left(M^2 - s^2\right)^{1/2}\right]^{1/2} \qquad \text{with} \qquad M = \frac{2s}{T_m} - \frac{s^2+1}{2}$$

Swanepoel, J. Phys. E: Sci. Instrum. 16, 1214 (1983)

Transmission spectrum fitting procedure (Swanepoel)

Legend:
- T_s
- T_M
- T_m

$$s = \frac{1}{T_s} + \left(\frac{1}{T_s^2} + 1 \right)^{\frac{1}{2}}$$
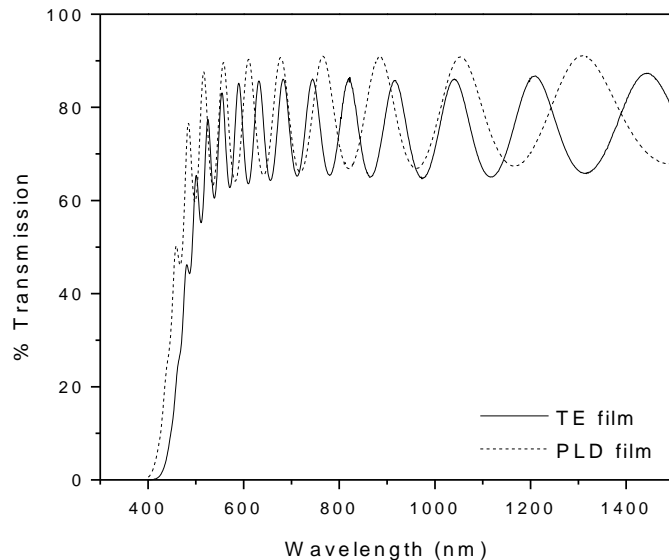
$$N = 2s \frac{T_M - T_m}{T_M T_m} + \frac{s^2 - 1}{2}$$

$$n = \left[N + \left(N^2 - s^2 \right)^{\frac{1}{2}} \right]^{\frac{1}{2}}$$

$$T_i = 2 \frac{T_M T_m}{T_M + T_m} \implies F = 2 \frac{8 n^2 s}{T_i} \implies x = \frac{F - \left[F^2 + \left(n^2 - 1 \right)^3 \left(n^2 - s^4 \right) \right]^{\frac{1}{2}}}{\left(n^2 - 1 \right)^3 \left(n - s^2 \right)}$$

$$\alpha = \frac{-\ln(x)}{d}$$

Refractive Index/Band Gap estimation from transmission spectra

Refractive index estimation
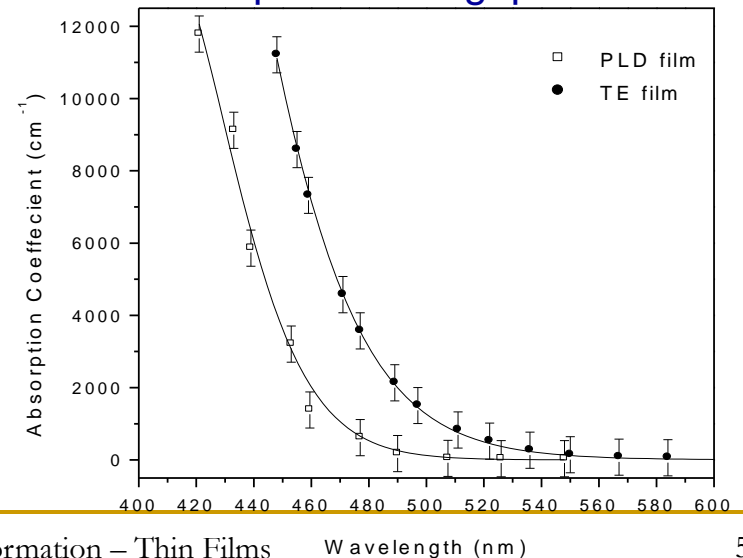
Transmission spectra of the films

• **Index of the films similar within error**

• **Absorption band gap of TE film is red-shifted compared to PLD film.**

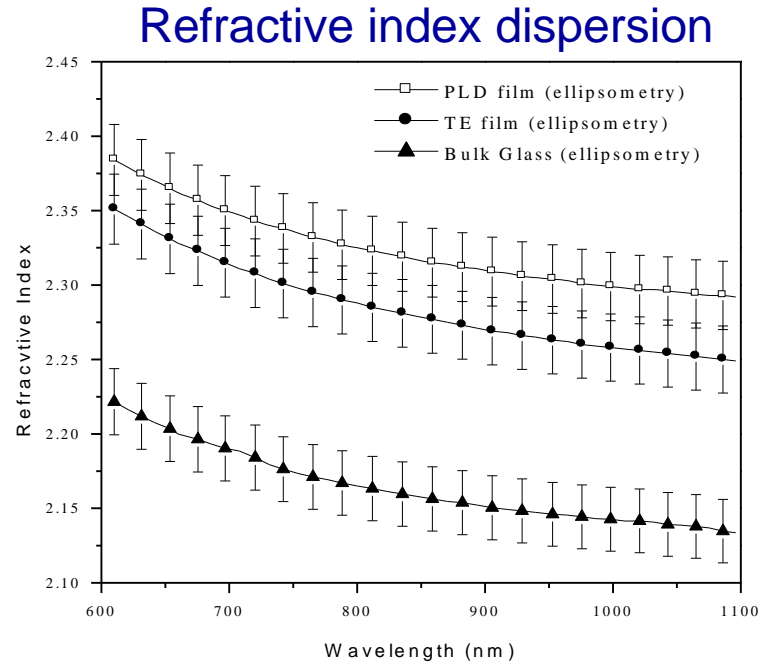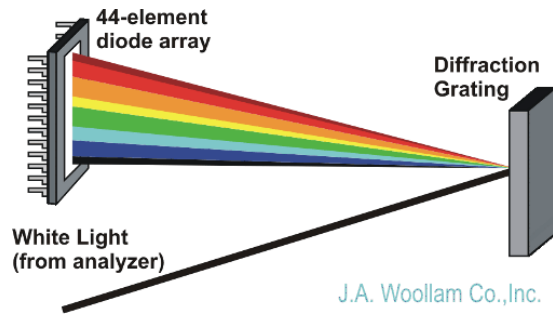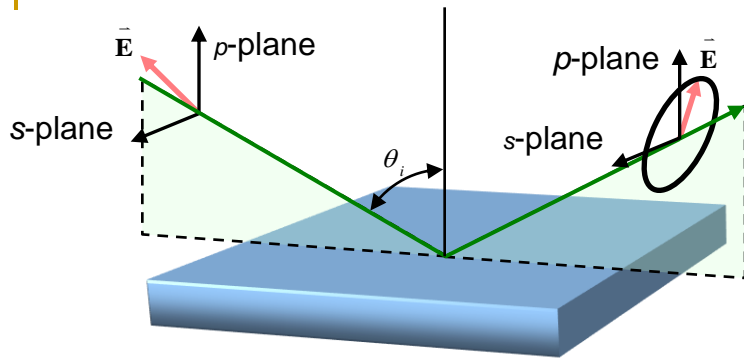• **Not possible to compare bulk values by this technique.**
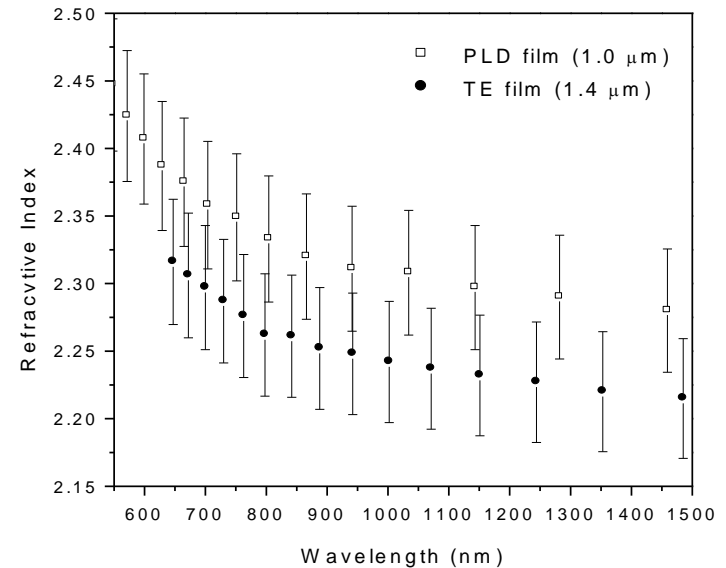
Absorption band gap estimation

Refractive index from Spectroscopic Ellipsometry

Refractive index dispersion

J.A. Woollam Co.,Inc.

$$R_p = \frac{\tan^2(\theta_i - \theta_t)}{\tan^2(\theta_i + \theta_t)} \quad R_s = \frac{\sin^2(\theta_i - \theta_t)}{\sin^2(\theta_i + \theta_t)}$$

$$\frac{n_1}{n_2} = \frac{\sin\theta_t}{\sin\theta_i} \qquad \rho = \frac{R_p}{R_s} = \tan(\psi)e^{i\Delta}$$

Optical model includes:
Simultaneous fitting at two angles (55 & 75)
Cauchy dispersion relation
Surface roughness layer (2-5 nm)

Correction for non-idealities:
Multiple internal reflections
Thickness non-uniformity (approx. 5%)
Spectral bandwidth (20 nm)

**Ellipsometry can confirm estimation of index from transmission spectra**

Ellipsometry to measure physical properties
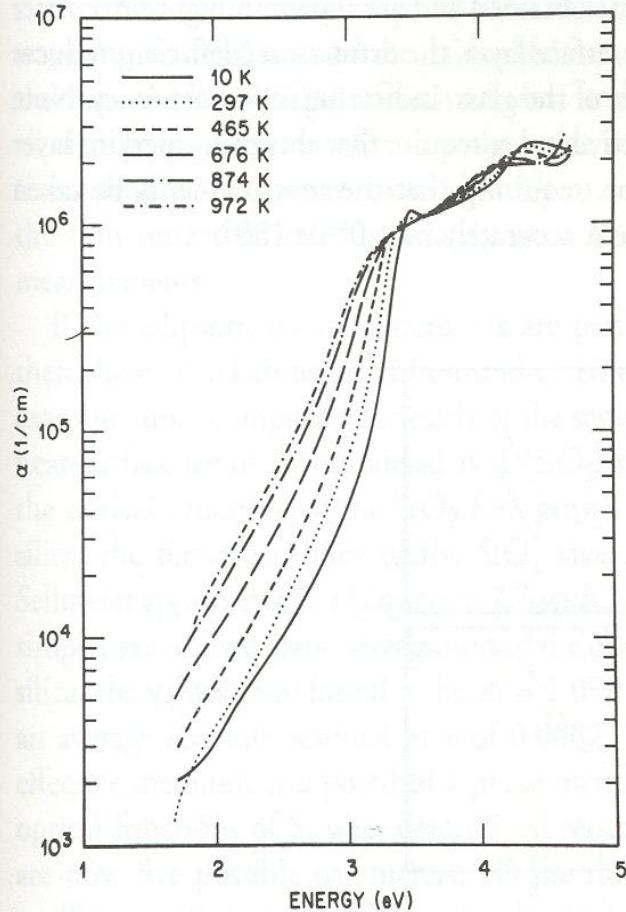
from G.E. Jellison, F. A. Modine Appl. Phys. Lett. 41 180-182 (1982)

Figure 2.2 The absorption coefficient of Si measured at several different temperatures using spectroscopic polarization modulation ellipsometry. (After Reference 21.)

Δn and n measurement of films

$$\phi = m2\pi$$
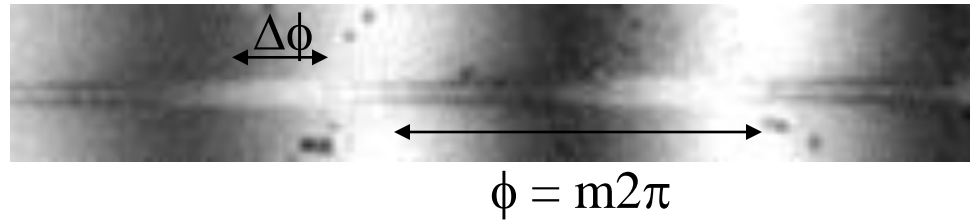
• Irradiation causes a change in the optical path through the sample

$$\frac{\Delta \phi}{2 \pi} = \frac{1}{\bar{\lambda}} \cdot 2 \Delta (OPD)$$

The factor of 2 is needed because the light travels through the sample twice

$$\Delta (OPD) = n_{irradiated} \, d_{irradiated} - n_{film} \, d_{film}$$

From prior measurements, we know:
- n_{film} - Transmission Spectrum
- d_{film} - Surface Profile with Zygo
- $d_{irradiated}$ - Photoexpansion from Zygo

thus, we can find $n_{irradiated}$ and the induced Δn

Refractive index measurement - films

The Δn value relates to the measured phase shift $\Delta\phi$ by:

$$\frac{\Delta\phi}{2\pi} = \frac{2d}{\lambda}\Delta n$$
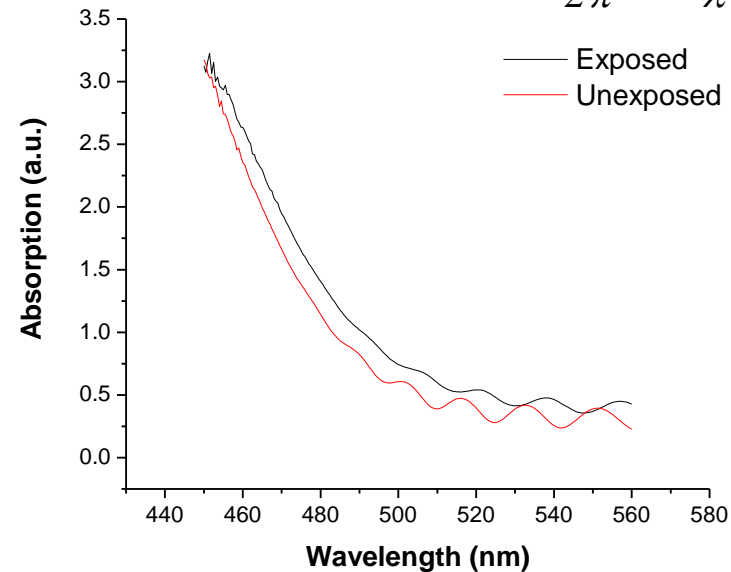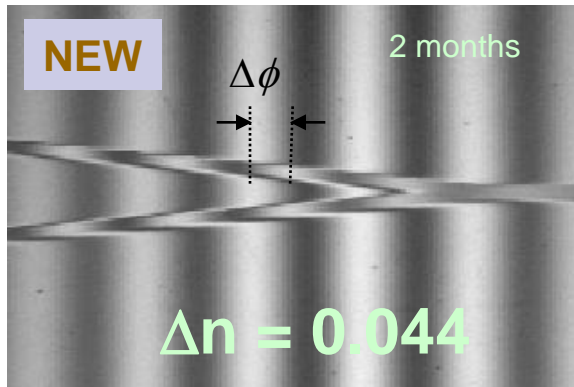

NEW   2 months

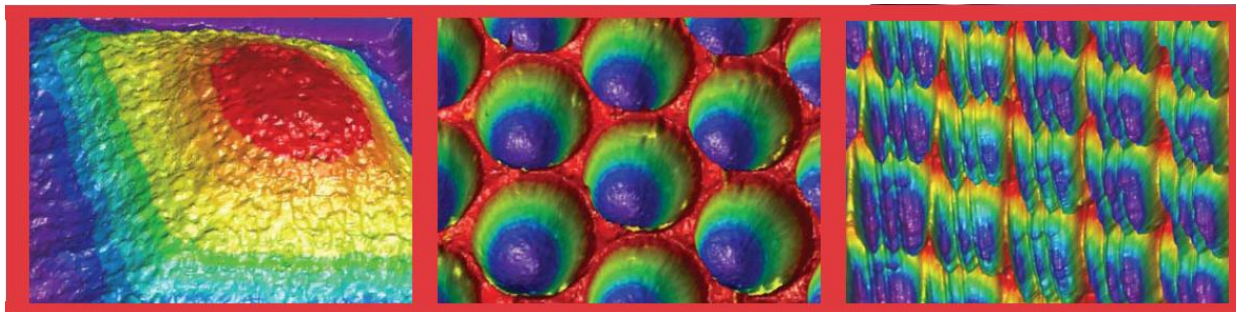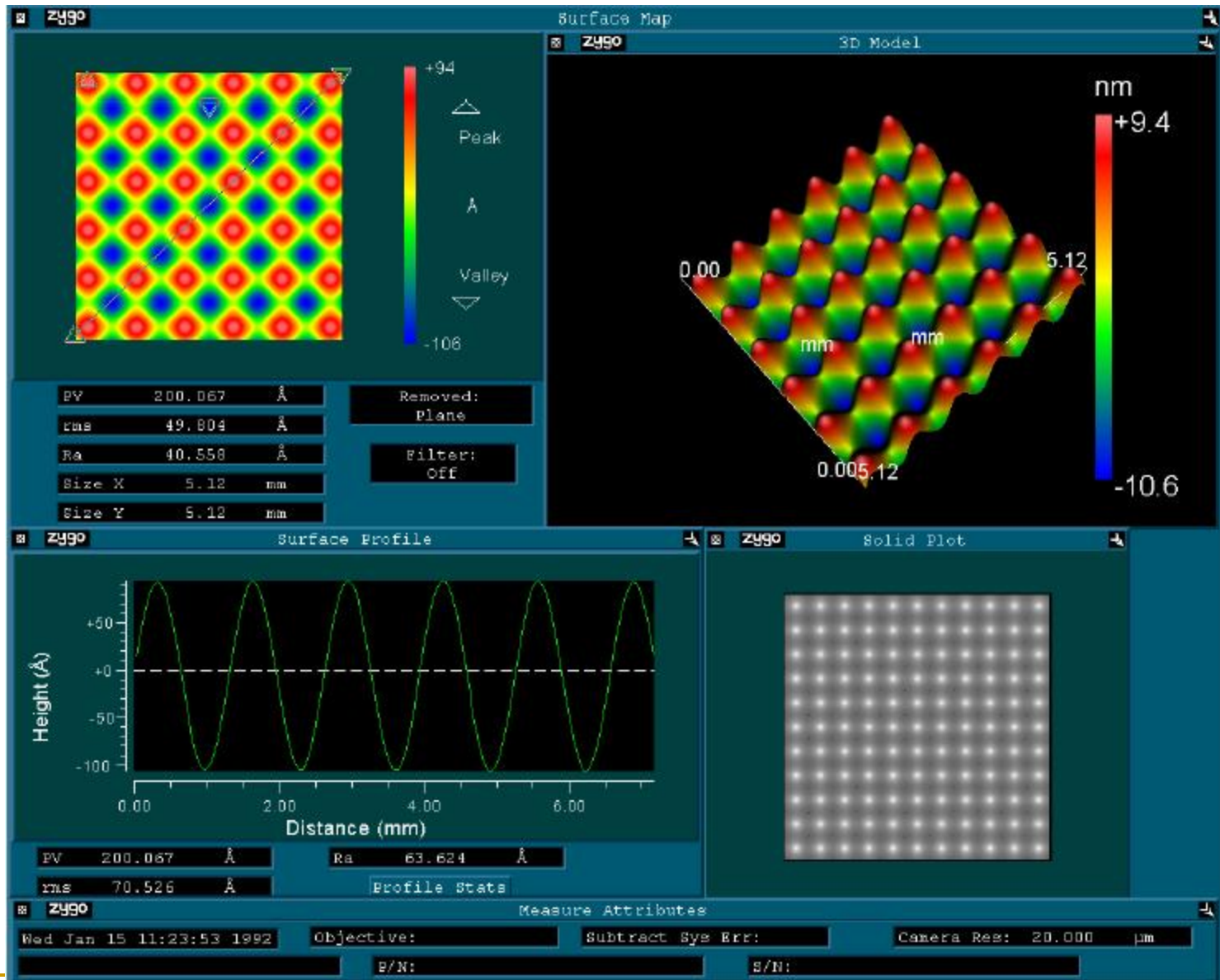$\Delta\phi$

$\Delta n = 0.044$

photo-darkening: increase of absorption and index upon exposure

Δn measurement: Interferometric method

- 3D optical profilometer
- 0.1 nm height resolution, independent of surface texture,
- submicron X-Y features reso
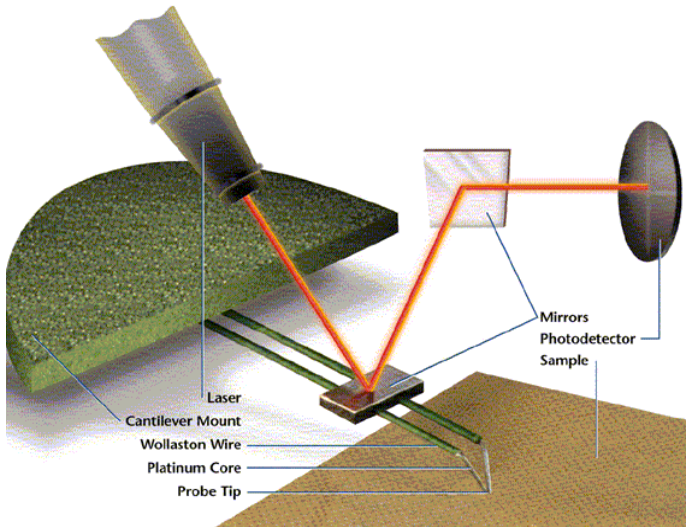- Profile areas up to 100 x 100 mm

Spatial surface characterization

Thermal properties from micro-thermal analysis

Sample Thermogram of PLD film

TA Instruments µTA-2990 Micro-thermal analyzer

Scanning area

Points for LTA
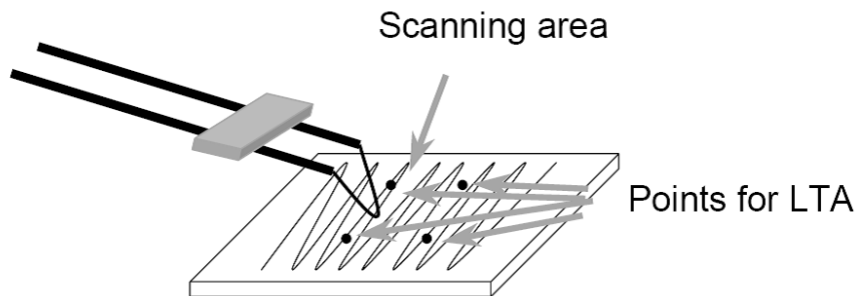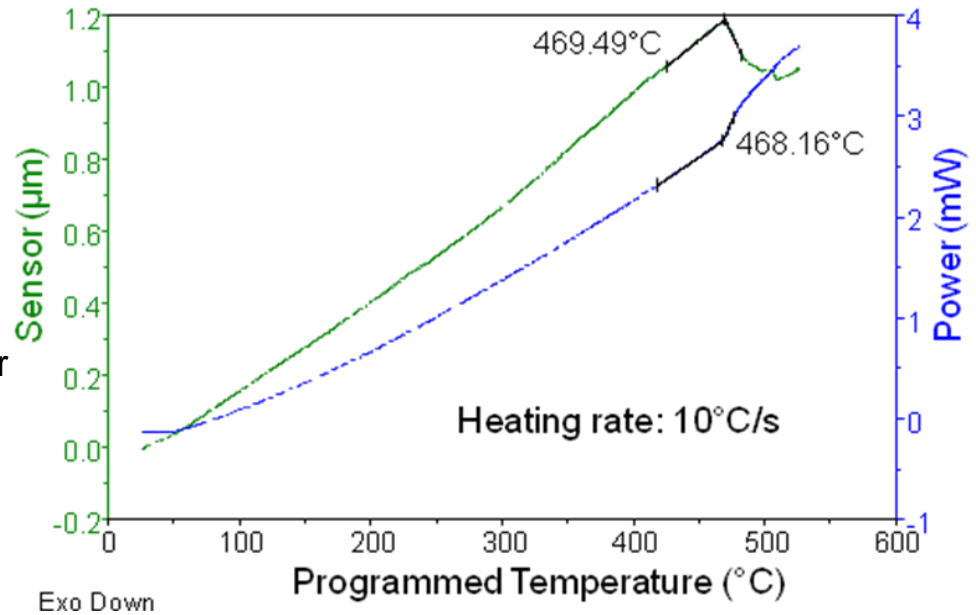
Probe penetration temperature is higher for films than for the bulk glass

μ-thermal analysis

- ## AFM tip
  - Surface topography
  - nm resolution
- ## Thermal tip
  - Local thermal analysis (transitions)
  - Thermal conductivity
  - Local thermal expansion
  - Maps of thermally-active defects
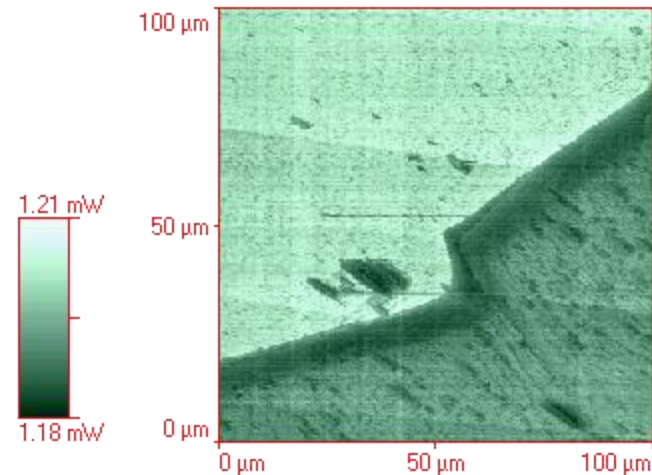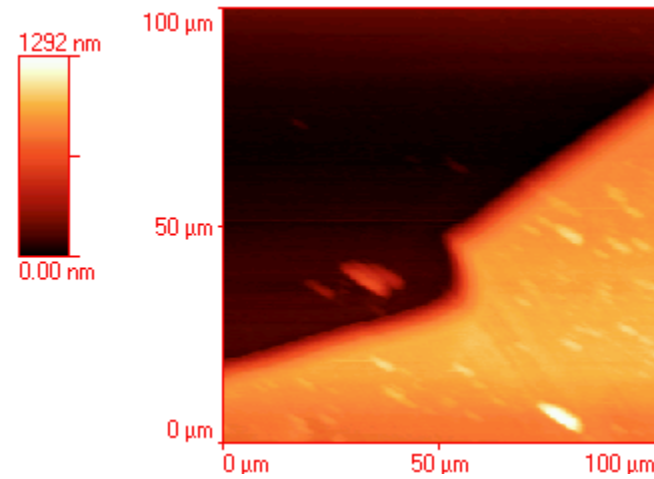
Thermal analysis of film

- AFM probe for topographic characterization
- Thermal probe for thermal characterization – requires reference
- Heating rates: 10C/sec (versus 10C/min)
- Film thickness and Substrate dependent (heat flow)
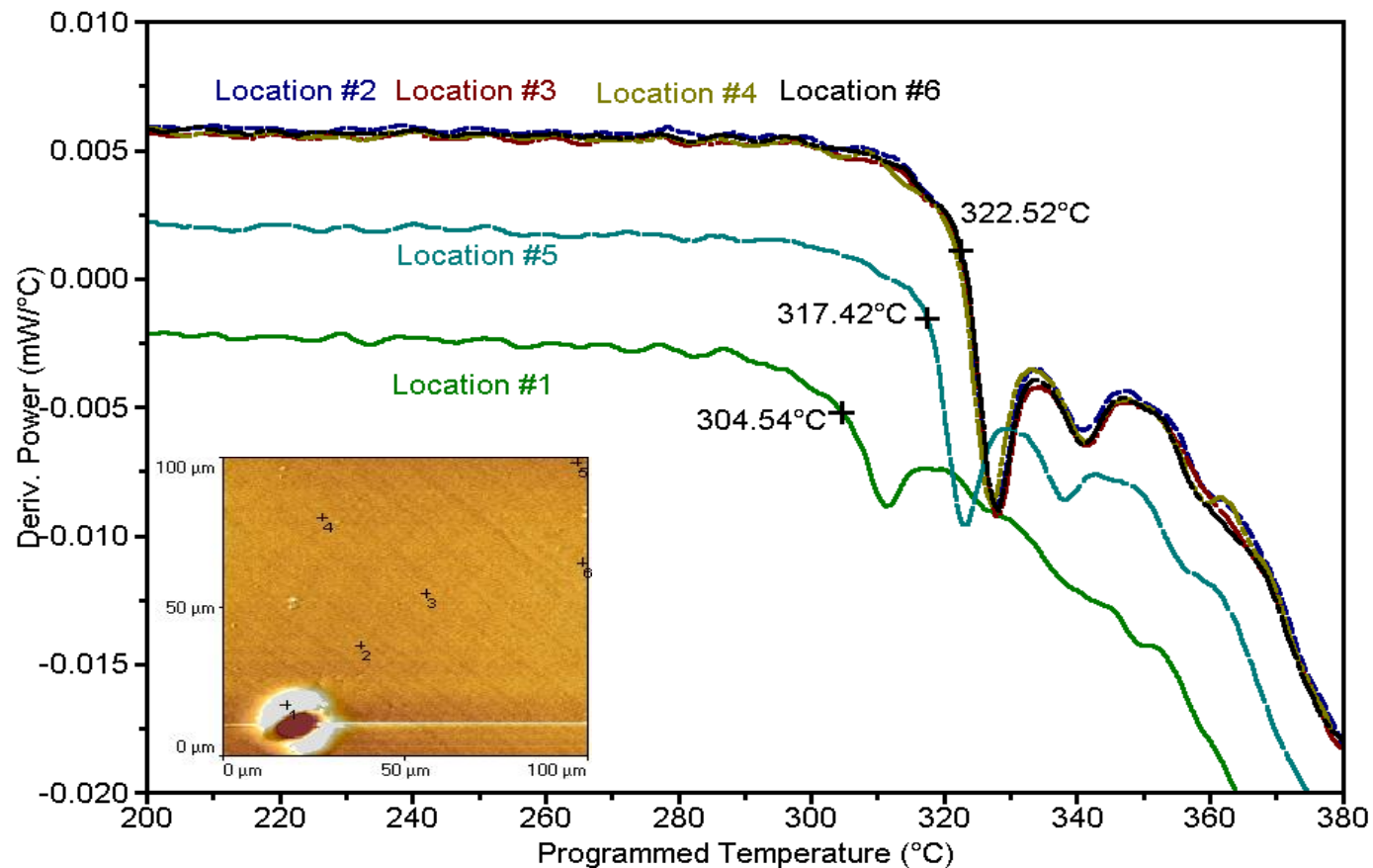
Laser written structures in As_2S_3 films

$I = 40$ GW/cm^2 ~ 10^6 pulses (a)

$I = 0.25$ GW/cm^2 ~ 10^6 pulses (b)

$\Lambda = 20$ μm

30 nm surface relief

(c)
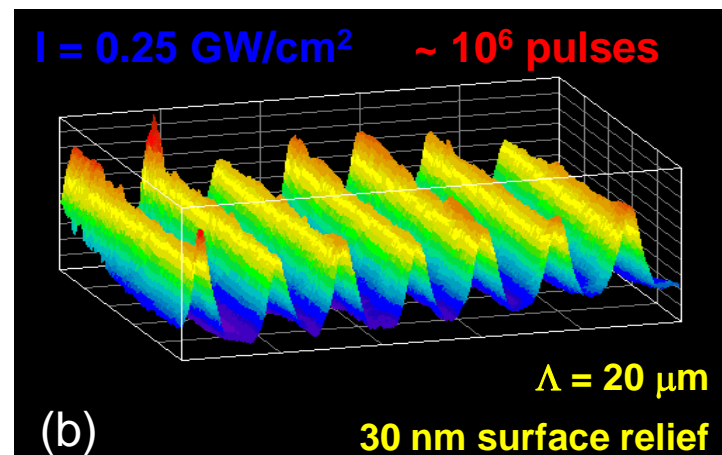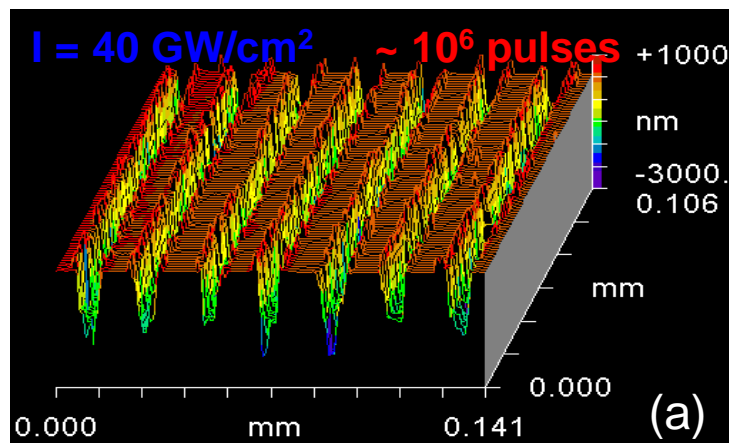
Surface profile (Zygo white light interferometer microscope)
(a) of a relief grating (10^6 pulses)
(b) of a phase grating (10^6 pulses)
(c) of a Y-coupler

Typical width ~10 μm (FWHM)

► **localized photo-expansion**

Ref: Microfabrication of waveguides and gratings in chalcogenide thin films, A. Zoubir et al.,Technical Digest. CLEO 2002, pp 125-126.
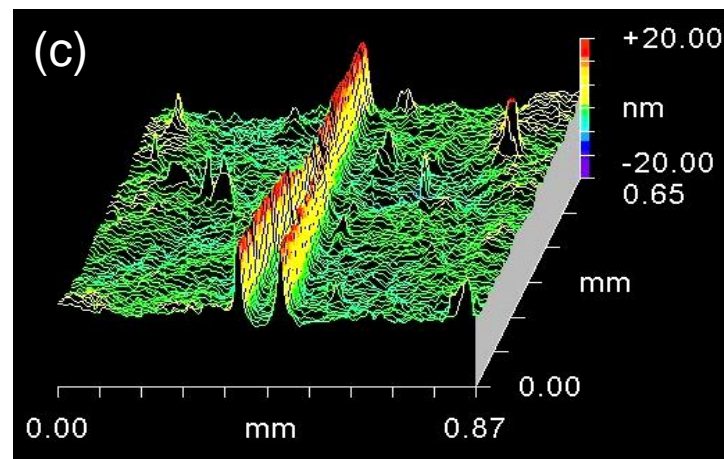
Micro-thermal analysis: characterization of laser-written structures

- As$_2$S$_3$ aged film; written with high intensity
- AFM analysis showed minimal surface relief
- μTA analysis shows an increase in thermal
  conductivity in same regions as the increase in
  refractive index
- fs-modification to local bonding arrangement leads to small variation in local thermal signal
- measurements being repeated on fresh films, freshly written structures.

Region of double-pass exposure during writing
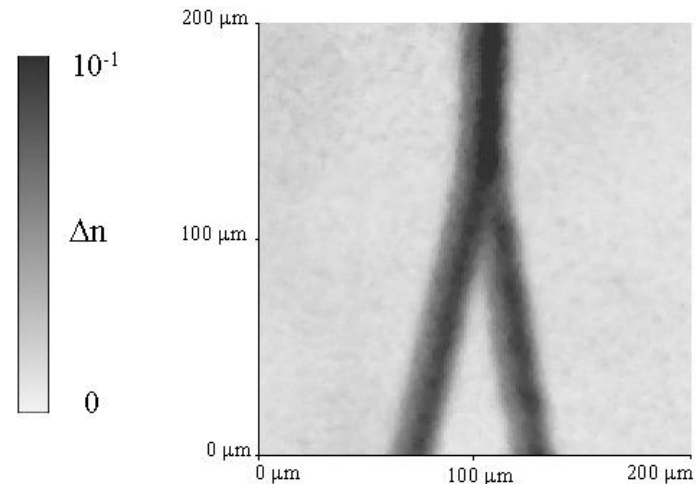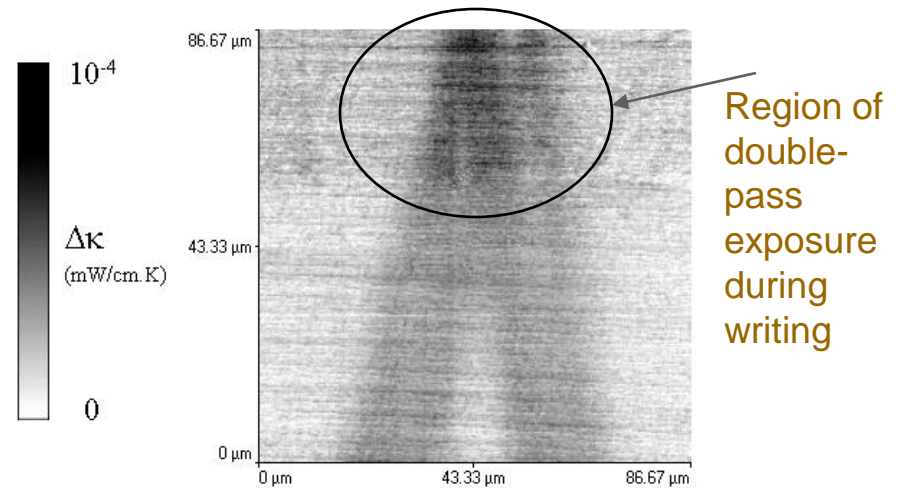
Characterization of the glass structure of the film

- **Raman spectroscopy**
- **Excitation source**
- **180˚ geometry**

to spectrometer / camera

polarized backscattered light

$\lambda = 752$ nm

incoming light

beam splitter

x100

sample

XYZ stage
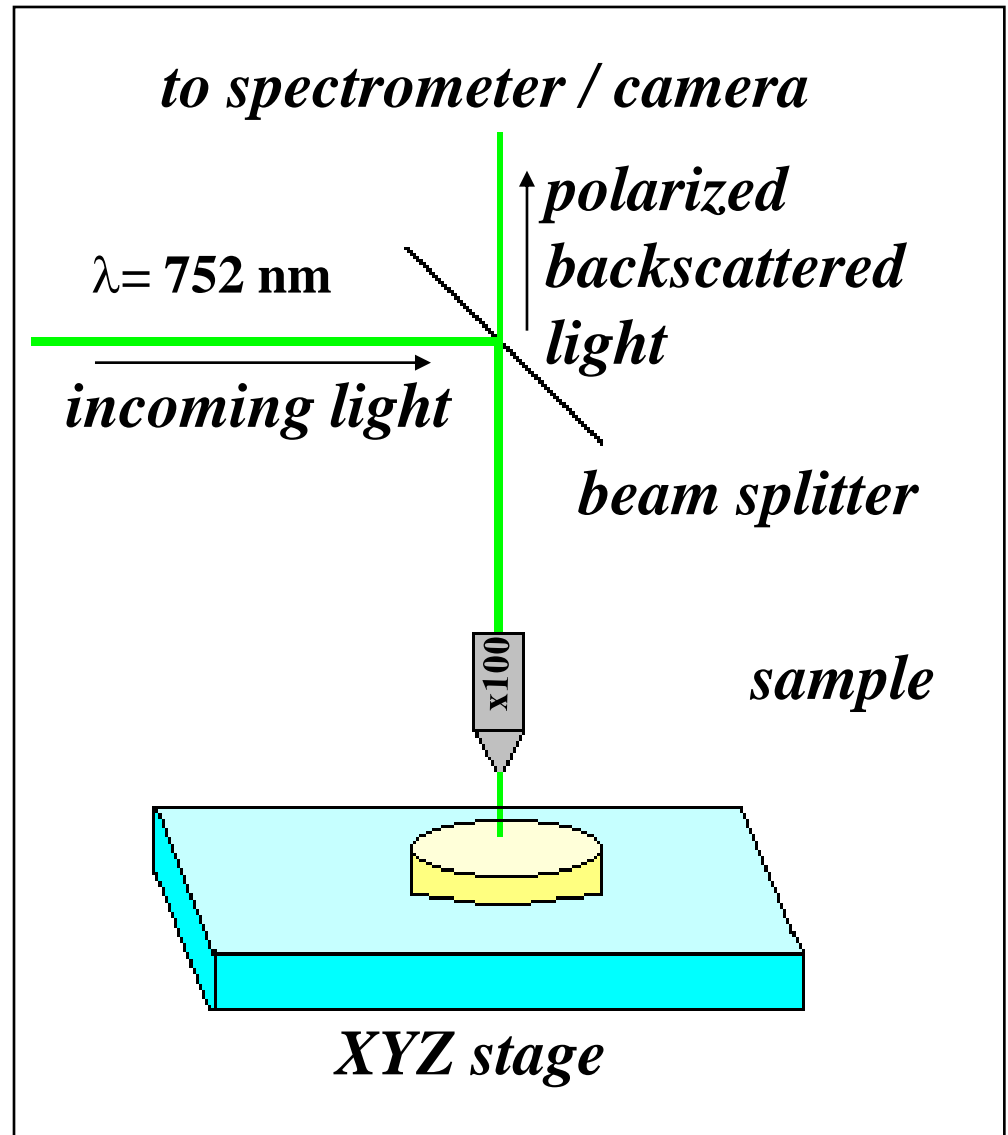
Raman Spectroscopy: fs-written bulk glass

10 μm

λ_{ex} = 632.8 nm
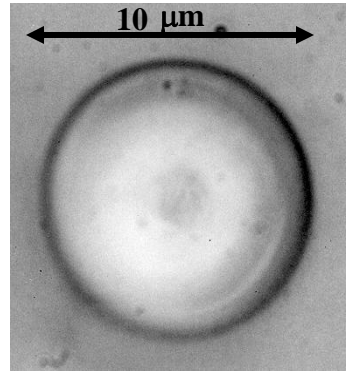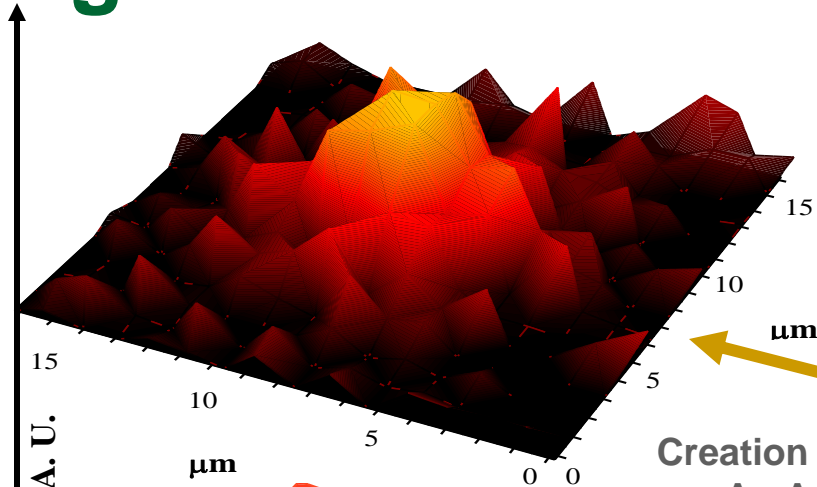
Creation of 236 cm^{-1}
As-As bonds
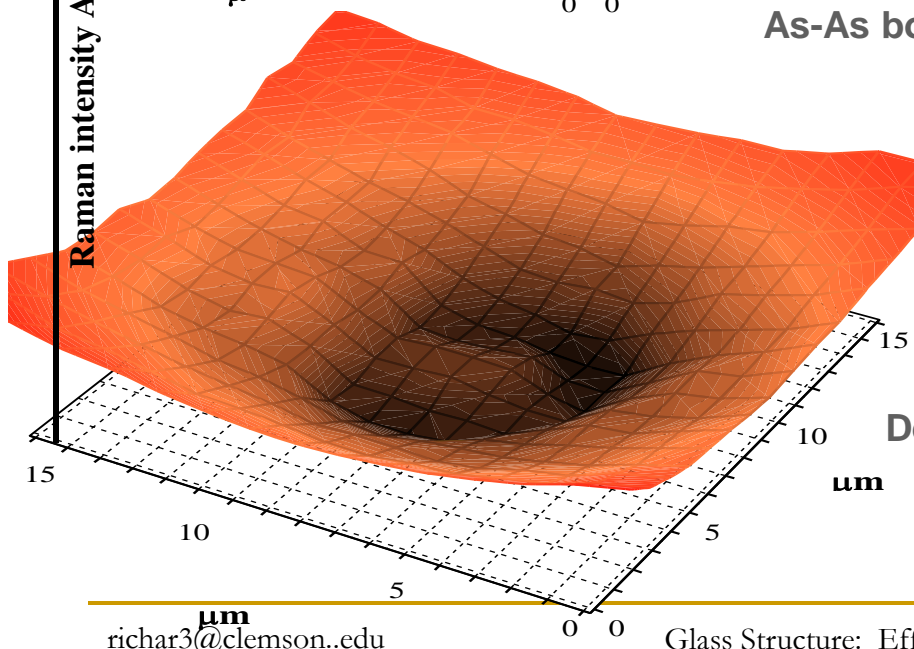
Depletion of 345 cm^{-1}
As-S bonds

Raman intensity A. U.

μm

As$_{36}$S$_{64}$

As$_{36}$S$_{64}$ exposed

As$_{40}$S$_{60}$

As$_{40}$S$_{60}$ exposed

As$_{42}$S$_{58}$

As$_{42}$S$_{58}$ exposed

200   400   600

Ref: "Waveguide writing in chalcogenide glasses by a train of femtosecond laser pulses," O. M. Efimov, et. al., J. Opt. Mater. 17 3 379-386, (2001)
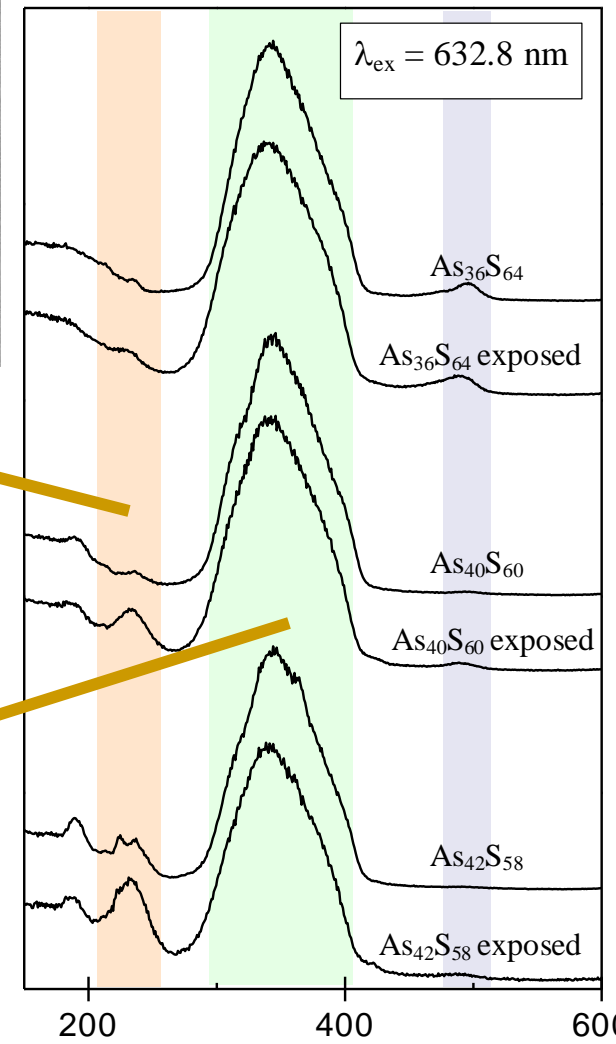
Waveguide Raman spectroscopy
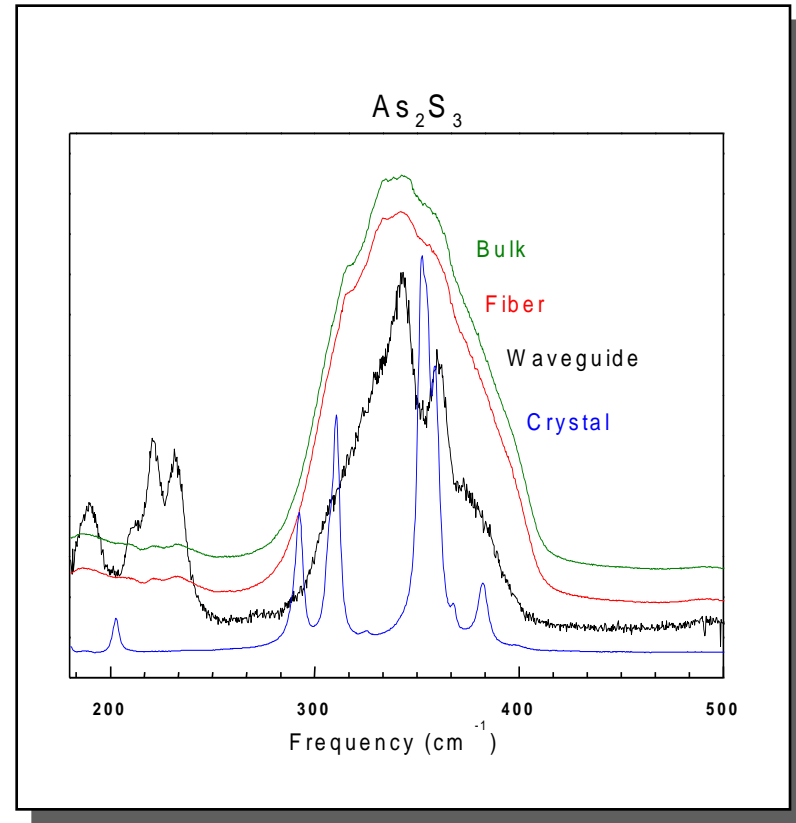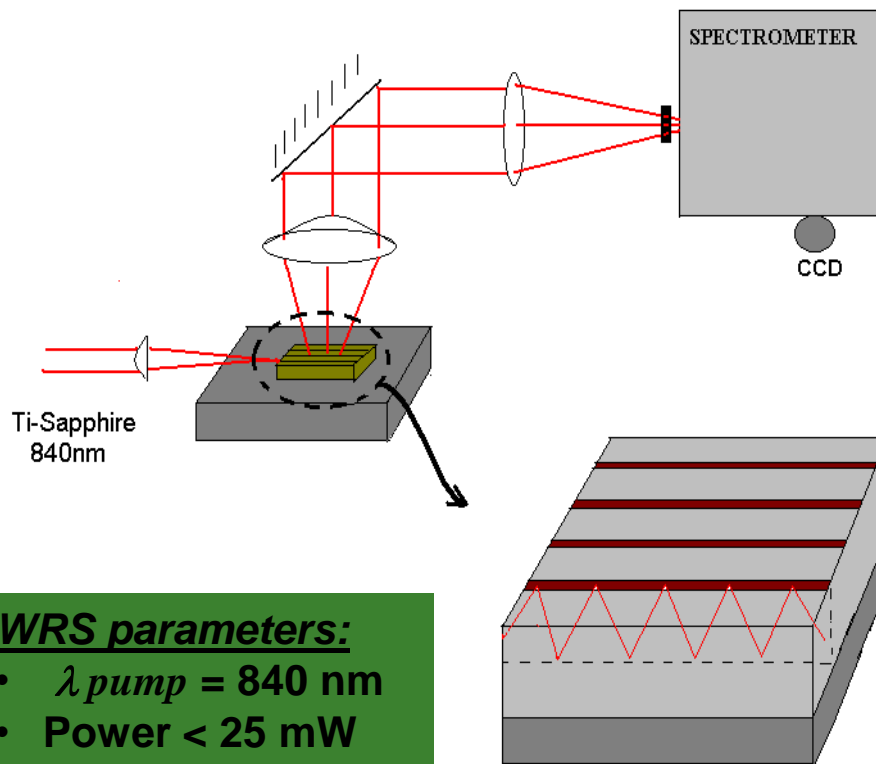
WRS parameters:
- $\lambda pump$ = 840 nm
- Power < 25 mW

- Ideally, As-S vibrations only (bulk); broad band centered at 345 cm^{-1}: vibrations in (As-S)$_{3/2}$ pyramidal sites
- Bulk and fiber: Small concentration of As-As (236 cm^{-1}) and S-S (494 cm^{-1}) bonds
- Waveguide (film) shows As$_4$S$_4$ molecular units and As-As, S-S bonds; no crystallinity

Bulk versus film: micro- vs WG Raman
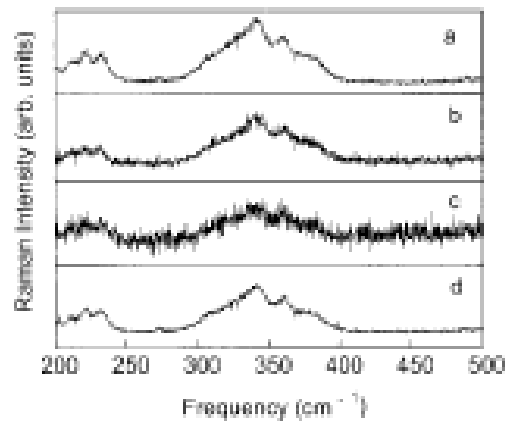
Figure 23.8: Waveguide Raman spectra of single layer, As$_2$S$_3$ channel structure. Panels (a) to (d) show a sequence traversing along the lateral direction (L to R) on the endface of the waveguide traversing from channel to channel. Excitation wavelength is 840 nm.

Effective coupling into the waveguide Is required to get film-specific structural information
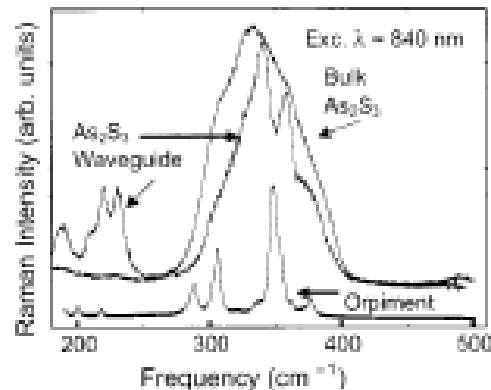
from "In-situ structural characterization of chalcogenide bulk-film-fiber properties by near-infrared waveguide Raman spectroscopy," A. Schulte, C. Rivero, K. Richardson, K. Turcotte, J. Laniel, V. Hamel, A. Villeneuve, A. Saliminia and T. Galstian, Optics Communications 198 125-128 (2001)

Figure 23.9: Structural features in film and bulk As$_2$S$_3$ Raman spectra as compared with high-purity crystal (from [66]). (Crystalline specimen courtesy of Prof. M. Frumar, University of Pardubice, Czech Republic).

Rutherford Backscattering Spectroscopy

The basis of RBS lies in the energy profile of ions that are backscattered from a sample. When a monoenergetic beam of ions is incident on a sample, a small fraction of the ions backscatter, and emerge from the sample at a reduced energy. The energy loss of the ions is due to interaction as they traverse in and out of the target material, and to the transfer of momentum that occurs during a single binary elastic collision (SBEC) with a target atom (Fig 2). By energy analyzing these rebounding ions at a given angle, a spectrum of events occurring throughout the volume of the sample is obtained. Application of conservation laws of energy and momentum translates this spectrum into sample composition as a function of depth.
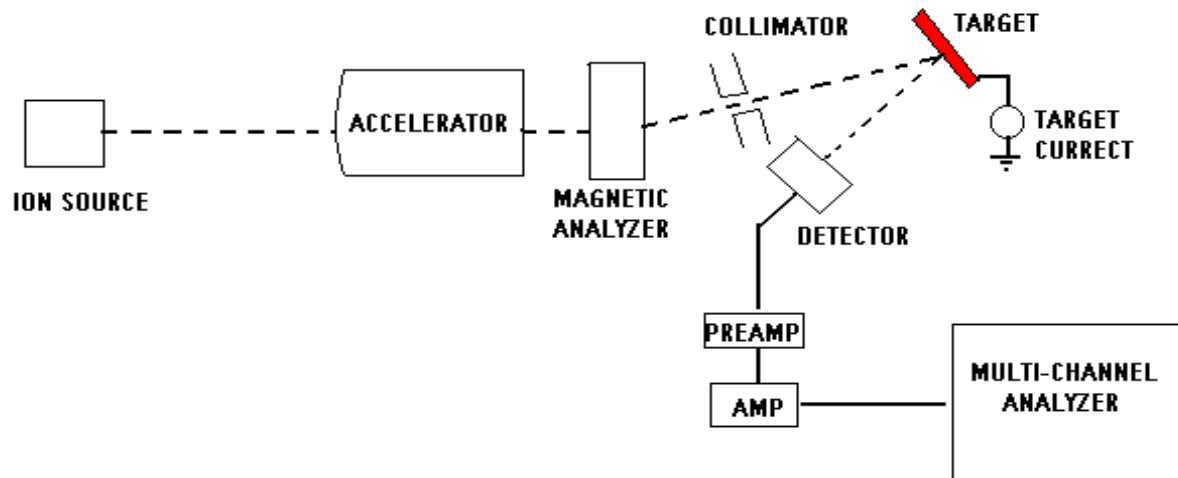
RBS: principles

By application of classical mechanics to surface collisions, the relationship of the mass M of the target atom, to the known mass m of the ion is defined by
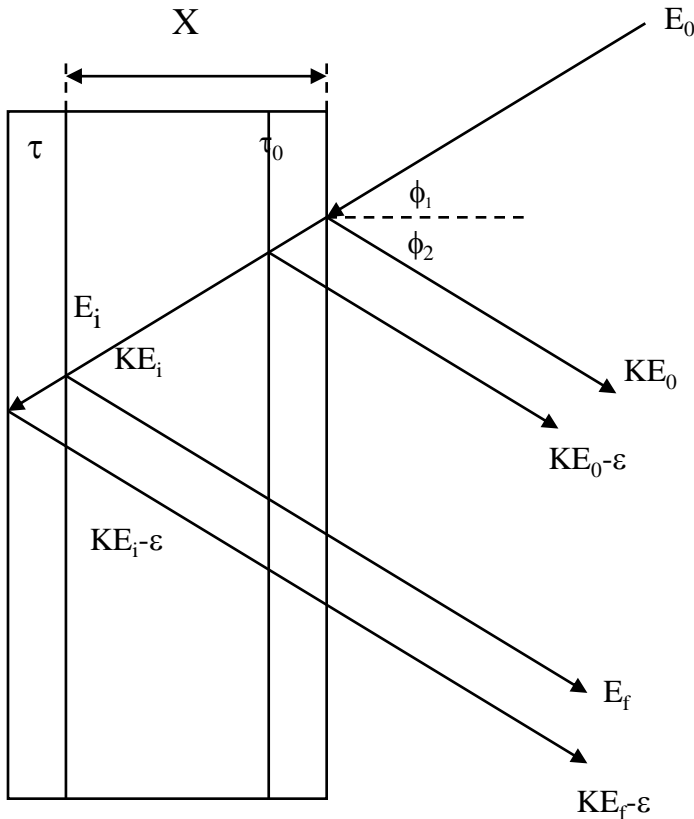
$$\frac{M}{m} = \frac{1 + E_f/E_i - 2\cos\theta\sqrt{E_f/E_i}}{1 - E_f/E_i}$$

Energies Ei and Ef denote the energy of the ion just prior and immediately after the collision, while θ ($\theta = 2\pi - \phi1 + \phi2$) is the angle from the incoming beam to the detector. The equation can be rearranged, giving Ef/Ei as a function of the mass of the target atom.

$$\frac{E_f}{E_i} = \left(\frac{\cos\theta \pm \sqrt{(M/m)^2 - \sin^2\theta}}{1 + M/m} \right)^2 = K$$

The ratio between Ef and Ei is defined as the kinematic factor, K. The kinematic factor is only a function of the scattering angle and the ratio of the target mass to the ion mass.

Principles, continued: how do we get compositional information

The stopping cross-section ε is fundamental to establish the change in energy, where N represents the atomic density of the target sample, x is the depth of the scattering event, and E_1 is the energy detected.

$$\Delta E = KE_0 - E_1 = [\varepsilon]Nx$$

The stopping cross-section and the differential cross-section (ε and σ, respectively) are figurative in analyzing the stoichiometry of the sample. The differential cross-section is determined by integrating over the solid angle of the detector, Ω.

$$\sigma \equiv \frac{1}{\Omega} \int_\Omega \frac{d\sigma}{d\Omega} d\Omega$$

The derivation of these equations from the classical mechanical theory gives an accurate estimation of the stoichiometry and density measurements proposed throughout this project. A more detailed analysis regarding the RBS theory is given in

A. C. Miller., R. B. Irwin, H. F. Helbig, "Low-Energy Ion Scattering and Rutherford Backscattering Spectroscopies", Physical Methods of Chemistry, 2nd edition, 9B, (1993)

RBS experimental conditions

The experiment employed a **1.7 MeV Tandetron Rutherford Backscattering System** which features a tandem accelerator. A helium ion beam was used to probe the sample. In a tandem accelerator, the source, which emits negative ions, is at ground potential. The negative ions are injected toward the positively charged terminal of the accelerator. He^+ ions are first generated from a duoplasmatron source. Extracted into a lithium charge exchange canal, a small fraction of the ions gain two electrons becoming He^{-1}. In the accelerator, the charge state of the ion is once again changed. Passing through a N_2 stripper gas cell, most of the ions are converted to He^{+2} resulting in repulsion from the positive terminal towards ground potential. The charge multiplication of the system, in transforming the He^{-1} to the He^{+2} ions, **allows for ion energies in excess of 5MeV**. The probe ion beam had a diameter of 1mm. Beam current at the target ranged from 18 to 20 nA, for each experiment. The sample was mounted with multiple axis goniometer control in a chamber evacuated to 7 x 10^{-7} Torr. The backscattered ions were detected using surface barrier detectors **at near-normal (165˚) and grazing incidence (100˚),** optimizing the mass and depth resolution, respectively. Pulses from the detector were formed and amplified by a pre-amp and amplifier and then subsequently distinguished by the multichannel analyzer.
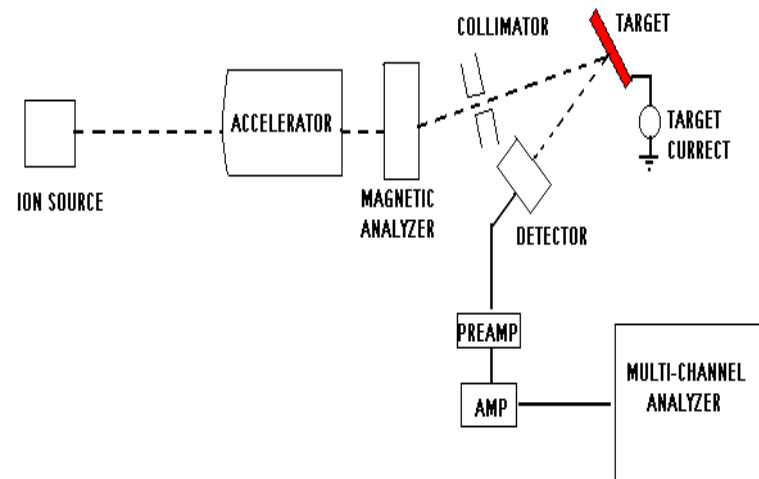
For additional info, see

A. B. Wittkower and H. D. Betz, At. Data, 5, 133 (1973) and

G. F. Knoll. "*Radiation Detection and Measurment*", 2nd ed., Wiley, New York, (1989)

RBS-example

1000 Å Ni film on Si
(Top) incidence of MeV ^{4}He ions on film
-Nearly all of the ^{4}He beam penetrates microns into the target before it is stopped
-Particles scattered from the front surface of the Ni have an energy given by the kinematic equation
$$E_1 = E_oK,$$

where the kinematic factor K for ^{4}He back-scattered at the incidence angle of 170° is 0.76 and 0.57 for Si

- As particles traverse the solid, they lose energy at a rate (64eV/ **Å**) ~ the Ni density (8.9 g/cm^3)

H is proportional to relative compositional fraction
Energy of peak is related to stopping energy and thickness
(bottom) reaction product Ni$_2$Si
ΔE_{Ni} has spread slightly owing to the presence of Si atoms contributing to the energy loss
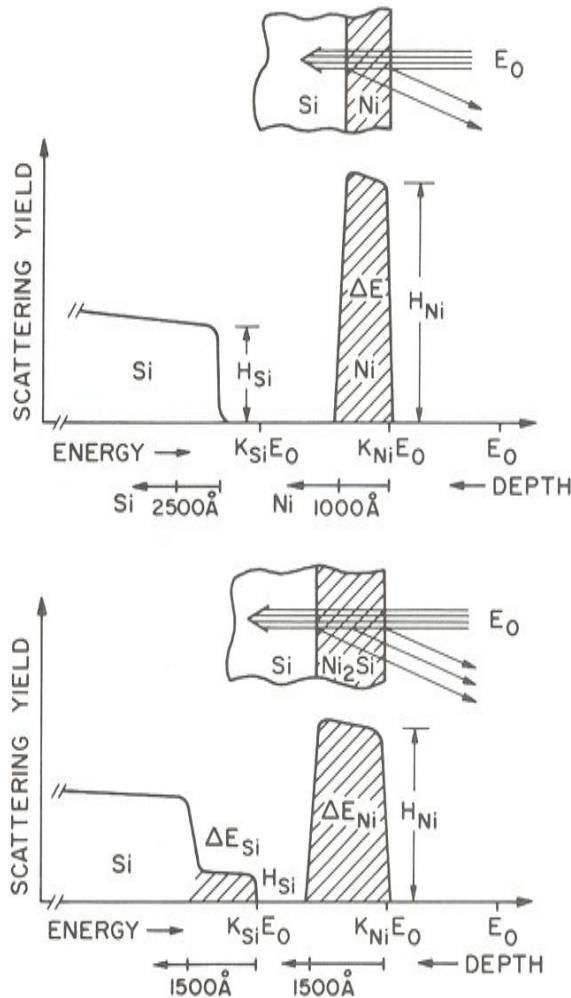The Si signal exhibits a step ~ Si in Ni$_2$Si

Figure 3.10 Schematic backscattering spectra for MeV ^{4}He ions incident on 1000 Å Ni film on Si (top) and after reaction to form Ni$_2$Si (bottom). Depth scales are indicated below the energy axes.

from Fundamentals of Surface and Thin Film Analysis, L. Feldman and J. Mayer, North Holland (1986)

Composition ratios from peak heights

- Ratio of heights H_{Ni}/H_{Si} of Ni to Si in the silicide layer gives the composition of the layer, by

$$\frac{N_{Ni}}{N_{Si}} \cong \frac{H_{Ni}}{H_{Si}} \frac{\sigma_{Si}}{\sigma_{Ni}} \cong \frac{H_{Ni}}{H_{Si}} \cdot \left(\frac{Z_{Si}}{Z_{Ni}}\right)^2, \tag{3.26}$$

where we have ignored the difference in stopping cross sections along the outward path for particles scattered from Ni and Si atoms. The yield from the Ni or Si in the silicide is given closely by the product of signal height and energy with ΔE. Therefore a better approximation to the concentration ratio of two elements A and B uniformly distributed within a film is

$$\frac{N_A}{N_B} = \frac{H_A \Delta E_A \sigma_B}{H_B \Delta E_B \sigma_A}. \tag{3.27}$$

In this case of Ni_2Si the difference between application of Eqs. (3.26) and (3.27) corresponds to a 5% difference in the determination of the stoichiometry of the silicide.

RBS conditions: damage

■ *Damage depth of probe ions*

RBS is considered a non-destructive profiling tool. High-energy He^{+2} ions probe the structure interacting primarily with the electron shells of atoms within the target. Most probe ions penetrate deep below the region of interest losing energy to electrons by inelastic collisions with little or no damage to the lattice, except for those very rare ions that are backscattered through large angles. **Almost all damage occurs near the end of range of the probing ions; approximately 17.3 μm into the silicon substrate in the case of 4 MeV He ions.**

see *http://www.TRIM.org*

Site repetition analysis (below) confirms the continued integrity of the film subsequent to analysis at 4 MeV. Here, **multiple measurements were made at the same site under identical probe conditions. Spectra reveal no displacement of constituent atoms within the sample following repeated analysis.** Radiation damage, although assumed nonexistent, would not be observable in the spectra.

Site Continuity on annealed Single Layer Sample
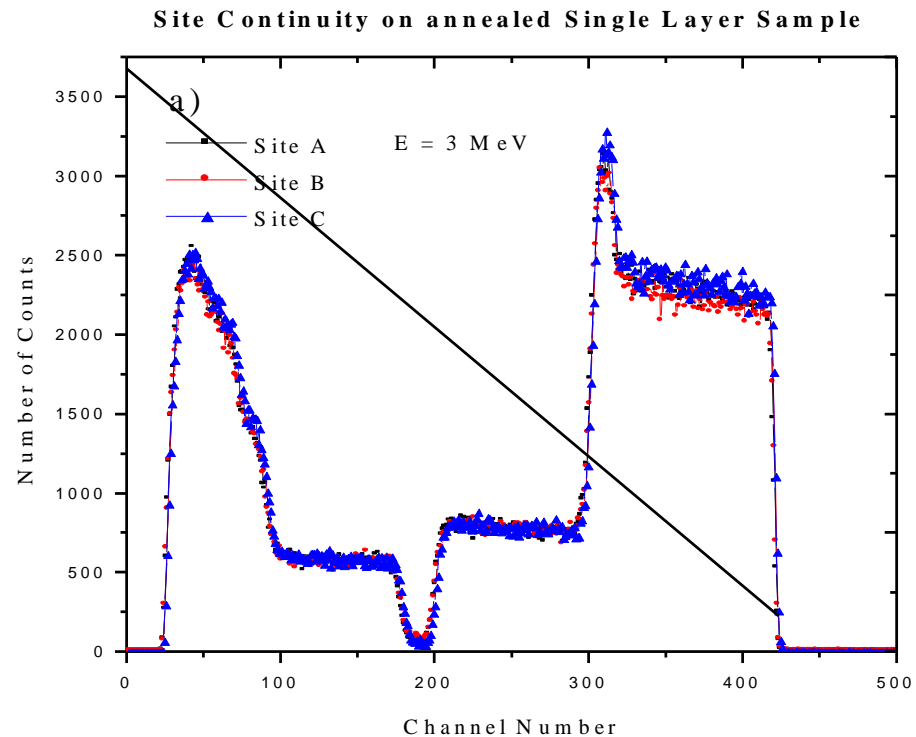
Results
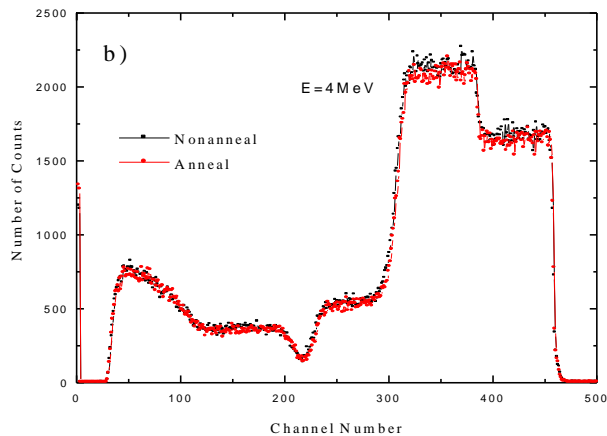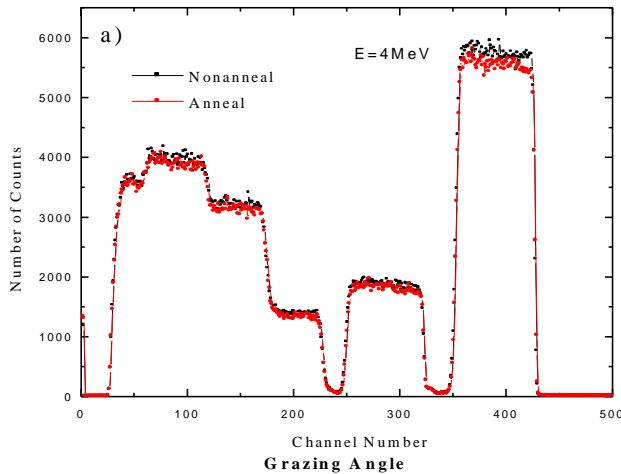
Normal angle spectra (top) and grazing angle spectra (bottom) of single layer As_2S_3 waveguide.

The common plateau width defined by the trailing edge of each species indicates their mutual existence in the compound layer. **Grazing angle spectra (bottom) confirms the elemental designation of the leading edges.** No variation in the density-thickness product is evident between the nonannealed and annealed samples. Density (ρ), was calculated based on a 1.66 μm layer thickness, t, determined using a Scanning Electron Microscope (SEM), where

$$\rho_{RBS} t_{RBS} = \rho_{REAL} t_{SEM}$$

The stoichiometry of the films was determined by taking the ratio of the parametric equation that defines the areal thickness, *A,* for each element (A & B), where the ratio m/n, represents the relevant abundance of element A and B (i.e. stoichiometry), given by:
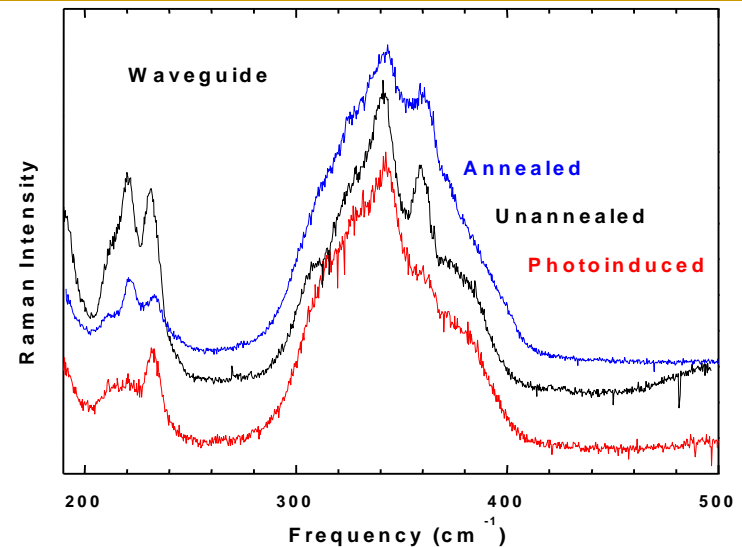
$$\frac{m}{n} = \frac{A_A \sigma_B (E_o)}{A_B \sigma_A (E_o)}$$

Results:

A measured As to S ratio, prescribing a 1.5 molar percent, was used to produce the bulk glass [$As_{0.4}S_{0.6}$]. RBS analysis of annealed and nonannealed films (below) are comparatively **sulfur-deficient** with respect to the original parent glass composition (often seen in thermal deposition). In addition, the RBS spectra show a slight density variation between the annealed and nonannealed structures; however, the discrepancy results within the deviation error presented by RBS analysis.

	Nonannealed	Annealed
Stoichiometry	$As_{0.416}S_{0.584}$	$As_{0.403}S_{0.597}$
Thickness (μm)	1.66	1.66
Density (g/cm^3)	2.93±10%	2.91±10%
% Uncertainty	0.65-1.12	0.68-1.11

Although variations in stoichiometry are within the experimental uncertainty, **it may also be assoc-iated with a reconfiguration of the molecular structure of the film during annealing**. As_4S_4 molecular clusters form during the thermal deposition of the films. These As_4S_4 sub-molecular features, represented by the sharp peaks in the Raman spectra, undergo reconfiguration with annealing and time. The near infrared Raman spectra show that the annealed and photoinduced waveguide have less As_4S_4 molecular clusters than the as-deposited structure. **These results imply that the variations observed in the Raman data are due only to a rearrangement of the molecular species in the glass matrix, which might induce modifications in the thickness (density) of the film, however it does not appear to affect the final stoichiometry of the film structure**.

*"In-situ structural characterization of chalcogenide bulk-film-fiber properties by near-infrared waveguide Raman spectroscopy," A. Schulte, C. Rivero, K. Richardson, K. Turcotte, J. Laniel, V. Hamel, A. Villeneuve, A. Saliminia and T. Galstian, Optics Communications **198** 125-128 (2001)*

Structural changes in glassy films

- **With composition**
- **With deposition condition**
    - **Target configuration, properties**
    - **Film deposition/formation rate**
- **With film age**
    - **Relaxation behavior**
    - **Stability of properties for device applications**
- **With external modification**
    - **Ion implantation (chemical changes)**
    - **Thermal history (cycling)**
    - **With induced optical modification**
        - **Photo-induced structural response**
        - **Need to know " before and after structure"**
        - **Assessment of bonding mechanism changes**

Lecture 24
Ends here